FLORIDA STATE UNIVERSITY

COLLEGE OF ARTS AND SCIENCES

THE SENSITIVITY OF REGIONAL CLIMATE SIMULATIONS OF CENTRAL AMERICA TO CHANGES IN CUMULUS PARAMETERIZATION

By

JUSTIN MICHAEL GONZALEZ

A Thesis submitted to the
Department of Earth, Ocean, and Atmospheric Science
in partial fulfillment of the
requirements for the degree of
Master of Meteorology

2025

Justin Gonzalez defended this thesis on March 5, 2025.

The members of the supervisory committee were:

Vasubandhu Misra
Professor Directing Thesis

Ming Cai
Committee Member

Michael Diamond
Committee Member

The Graduate School has verified and approved the above-named committee members and certifies that the thesis has been approved in accordance with university requirements.

ACKNOWLEDGMENTS

We acknowledge support from NASA grant 80NSSC22K0595. The IMERG dataset was provided by the NASA/Goddard Space Flight Center.

TABLE OF CONTENTS

LIST OF TABLES

LIST OF FIGURES

ABSTRACT

Central America is challenging to simulate through numerical modeling due to its complex geography and climate modulators. Therefore, it is worth evaluating how the usage of different physical schemes can affect our ability to simulate the regional climatology and its variations. In this study, two coupled ocean-atmosphere regional climate simulations that differ only in their cumulus parameterization schemes (RR-RAS and RR-KF2) are compared and verified over 16 years, at 15 km grid spacing, and centered over Central America. Both model integrations are forced at the lateral boundaries with identical atmospheric and oceanic reanalysis. The Relaxed Arakawa Schubert (RAS) scheme is based on quasi-equilibrium theory, while the Kain-Fritsch (KF2) scheme is based on an entraining/detraining plume model, which triggers convection upon reaching a CAPE and moisture convergence threshold. The RR-KF2 scheme shows several notable improvements in the simulation relative to the RR-RAS scheme. These include a reduction of the terrestrial wet bias, the dry bias of the atmospheric column over the oceans, biases in the low-level wind field, and coastal cold SST bias, alongside an improved representation of the ITCZ location in the eastern Pacific Ocean, convective rainfall within coastal and terrestrial points, thermocline depths in the Caribbean Sea, and generation of upward oceanic heat fluxes. Despite these advancements, the bias in RR-KF2 simulations is still large and significant, with a considerable terrestrial wet bias, absent stratiform precipitation over regions of deep convection of open ocean, a weak ITCZ, warm SST biases in the open ocean, and a shallow thermocline bias in the Caribbean Sea among those remaining. Changes in the climatology when adopting RR-RAS or RR-KF2 can relate to their simulated convection due to qualities such as the cloud radiative effects and/or wind field changes. It is encouraging to note that both simulations produced diurnal rainfall variability, with their amplitude and phase verifying reasonably well with corresponding observations. RR-RAS and RR-KF2 similarly verified the differences in amplitude between the Pacific and the Caribbean coasts for the Mid-Summer Drought; however, the models over-amplified the biannual rainfall peaks relative to observations. As this study reveals, while adopting the KF2 cumulus parameterization scheme shows promise, work is still needed to resolve these biases and enhance the fidelity of regional climate simulations of Central America.

CHAPTER 1

INTRODUCTION

1.1 Precipitation Climatology of Central America

Central America is an isthmus that stretches diagonally from Guatemala in the northwest to Panama in the southeast, connecting the North and South American continents. Much of this region is separated by the continental divide into a Caribbean and a Pacific slope, each bordered by a large warm body of water. On an annual scale, the Central American climate oscillates between a dry and wet phase in which each slope of the isthmus contains distinct seasonal patterns (Alfaro 2002; Amador et al. 2006, 2008; Wang et al. 2014; Hidalgo et al. 2015; Sáenz et al. 2023). The EOF analysis of Fig. 1 from Alfaro (2002) exemplifies how these seasonal fluctuations manifest into two dominant patterns: a Pacific regime and a Caribbean regime.

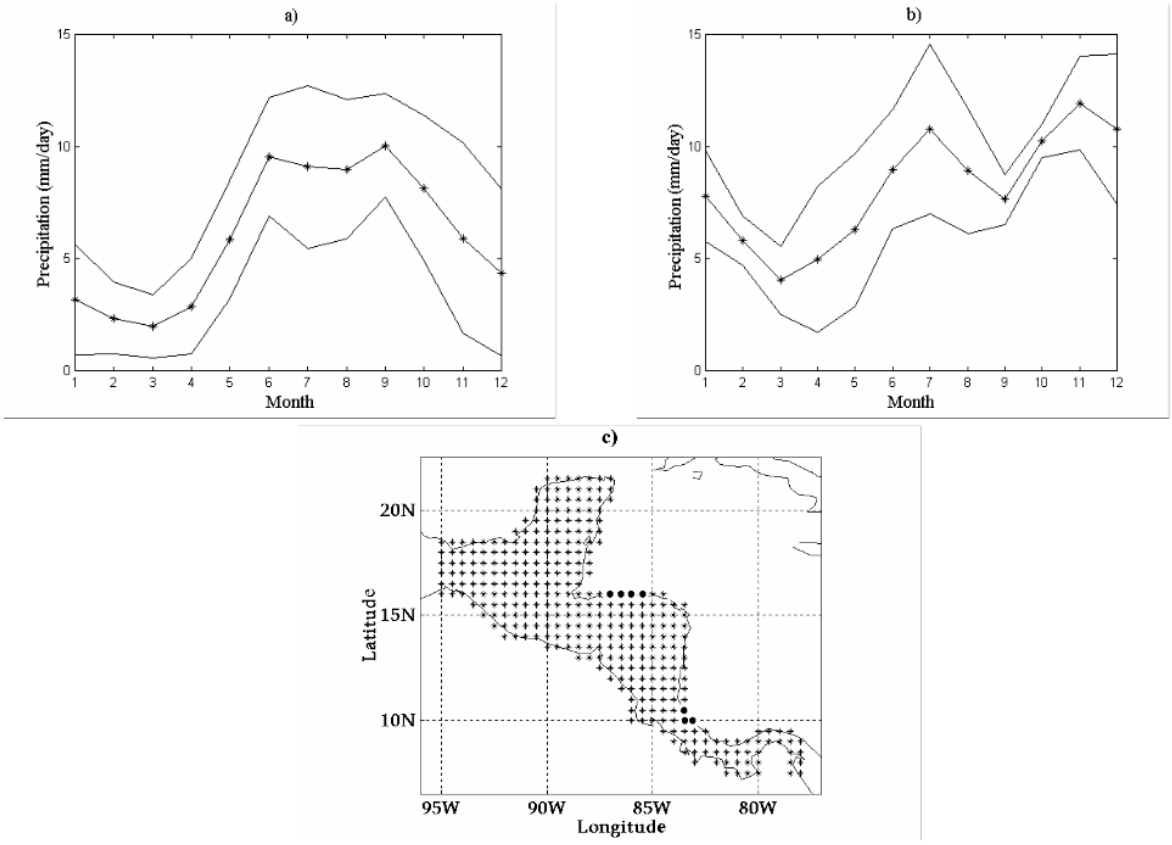

Figure 1: EOF analysis of precipitation climatology over Central America. Panels a and b display the two dominant annual cycle patterns, which are the Pacific and Caribbean regime respectively. Panel c displays the domain used for the EOF analysis. From Alfaro (2002).

Along the Caribbean slope, precipitation maintains a consistent presence throughout the year, with the highest precipitation seen in boreal winter and summer and the lowest seen in boreal spring and fall. These maxima and minima coincide with the seasonal changes in the strength of the Caribbean Low-Level Jet (CLLJ; Davis et al. 1997; Amador et al. 2006, 2008; Muñoz et al. 2008; Durán-Quesada et al. 2017; Hidalgo et al. 2015; Sáenz et al. 2023). The CLLJ forms from the meridional sea-level pressure gradient established by the North Atlantic Subtropical High, further enhanced by the meridional temperature gradient between the relatively warm Greater Antilles and the cool Caribbean Sea. The climatological strength of the CLLJ is highest during July and February, hence the wettest portions of the year for the Caribbean slope occurring during those respective seasons. During these periods, rainfall is enhanced through Caribbean moisture transport and bolstered lifting within the CLLJ exit region and windward mountain slopes. Conversely, the meridional sea-level pressure gradient is weakest during the boreal spring and autumn, causing the CLLJ to weaken, enabling the precipitation minima during those seasons.

The Pacific slope of Central America has its wet season throughout the boreal summer and fall and dry season during the boreal winter and spring, with the seasonal movement of the Inter-Tropical Convergence Zone (ITCZ) being the primary driver of this pattern as it alternates between its northernmost and southernmost position respectively (Amador et al. 2006, 2008; Hastenranth and Polzin 2013; Hidalgo et al. 2015; Sáenz et al. 2023). However, it is worth noting that factors beyond the ITCZ significantly control precipitation for the Pacific slope, one such feature being the Mid-Summer Drought (MSD; Magaña et al. 1999; Amador et al. 2006, 2008). During July and August, the Pacific slope of Central America experiences a local minima of rainfall amid the rainy season; this phenomenon is the MSD, locally referred to by distinct names such as veranillo or canícula. Before the MSD onset, warm SSTs throughout the eastern tropical Pacific found in May and June enable organized convection, such as that found in the ITCZ. This frequent and widespread convection blocks incoming solar radiation, causing a gradual cooling of SSTs. Once July and August arrive, SSTs cool enough to enable the growth of an anomalous anticyclonic circulation off the Pacific coast of Mexico, causing easterly winds from the CLLJ to accelerate and bring widespread subsidence as they flow over the continental divide, suppressing thunderstorm development along the Pacific slope. During this period, the MSD is most prominent in the Central American dry corridor, along the Pacific littoral from Western

Guatemala through northern Costa Rica (Gotlieb et al. 2019). Near the start of boreal fall, SSTs warm enough from incoming shortwave radiation that convection returns, and the demise of the MSD follows. The variability in MSD has key agricultural and economic consequences for the region, meaning it is imperative to have an accurate simulation of this feature along with the ITCZ to predict how it may change with a warming climate (Hidalgo et al. 2019; Stewart et al. 2022).

Furthermore, the Choco Jet (CJ) is a moisture belt for the Pacific slope during the boreal fall, particularly in October and November (Poveda and Mesa 2000; Amador et al. 2008; Durán-Quesada et al. 2017). The CJ, first identified by Poveda and Mesa (2000), forms from the southerly cross-equatorial flow of the ITCZ. As these winds cross the equator, they turn toward the east as the Coriolis force direction changes, and friction acts upon them. Additionally, a zonal temperature gradient between the warm landmass of Colombia and the eastern tropical Pacific Ocean strengthens these winds through the thermal wind relation, creating the CJ. The CJ transports moisture and enables topographic lift as it reaches the southern end of the Pacific slope, enhancing rainfall alongside the ITCZ. Much of the moisture transport climatology in Central America can be understood as a see-saw mechanism between the CLLJ and CJ, in which one jet transports moisture to the landmass when the other wanes in strength (Durán-Quesada et al. 2017). In the winter and summer, the CLLJ brings moisture from the east to the Caribbean slope, enabling widespread precipitation in this region while suppressing rainfall along the Pacific slope as its easterly winds flow over the continental divide and into the east Pacific Ocean. In autumn, as the CLLJ enters a weakened state, the CJ becomes dominant as it brings moisture from the south and west into the Pacific slope.

Beyond the CLLJ and CJ, other LLJs play a key role in modulating the Central American climate system through various air-sea interactions such as enthalpy fluxes and ocean mixing. These LLJs include the Papagayo Jet (PaLLJ), a northeasterly jet off the Pacific coast of Nicaragua and Costa Rica; the Panama Jet (PJ), a northerly jet within the Gulf of Panama; and the Tehuantepec Jet (TeLLJ), a northerly wind jet originating from the Isthmus of Tehuantepec. These additional jets are primarily prominent in the winter and spring seasons (Fielder 2002; Muñoz et al. 2008; Misra and Jayasankar 2022). For clarity, the schematic below (Fig. 2) includes a sketch of the geographical locations of each of these LLJs and their general wind patterns.

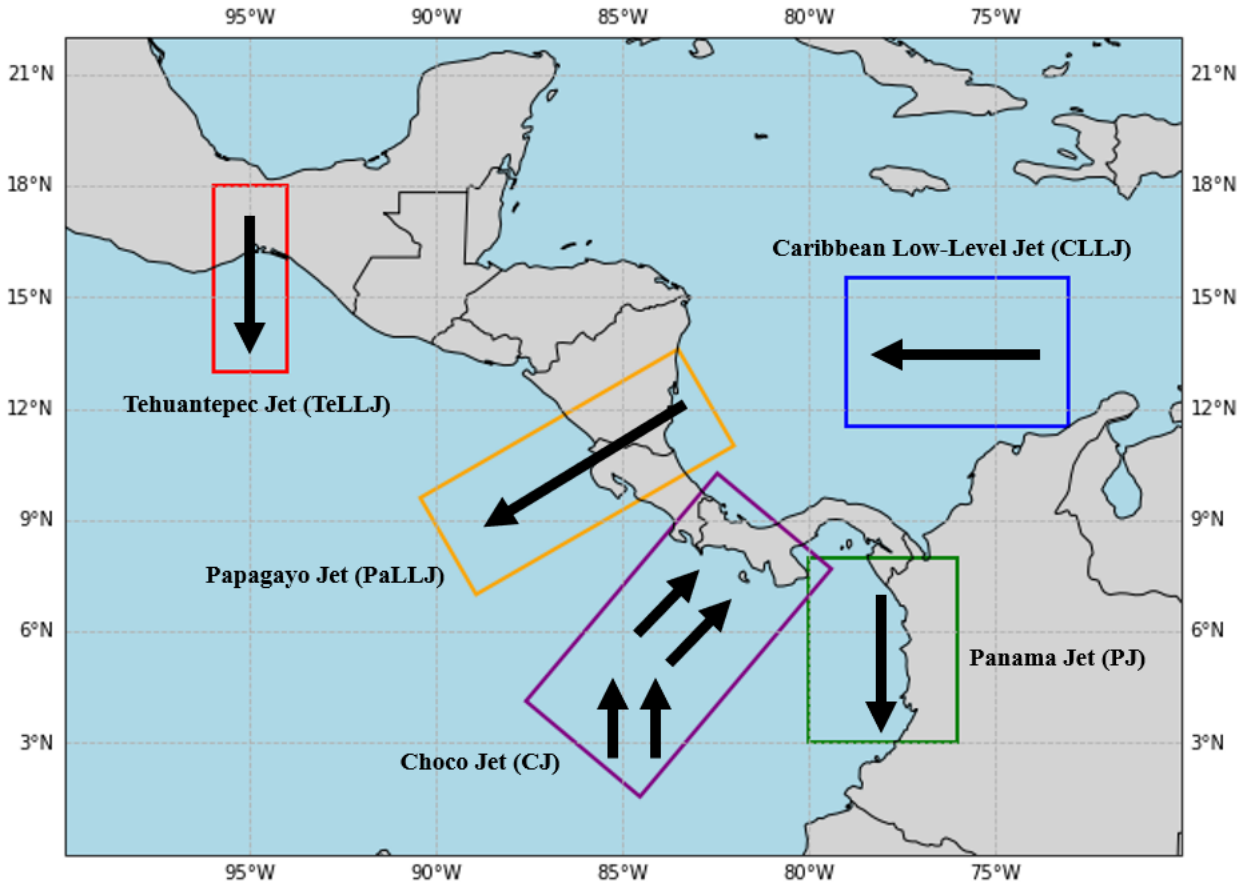

Figure 2: Schematic of general locations and wind directions of each LLJ in Central America. MJ22 and Poveda and Mesa (2000) were used to obtain the approximate locations for these domains.

Diurnal rainfall variability, another facet of Central America's climate, is primarily controlled by land-sea interactions, which are most prominent in the boreal summer, making this period the focus of this work and previous literature (Garreaud and Wallace 1997; Mapes et al. Part 1, Part 3 2003; Curtis 2004; Vera et al. 2006; Diro et al. 2012). Observational analysis, such as that of Curtis (2004), reveals an alternating pattern in which diurnal rainfall over the Central American landmass contains nocturnal peaks (18:00 to 03:00 h LST) while the eastern Pacific contains daytime peaks (06:00 to 15:00 h LST). These results were further affirmed by Diro et al. (2012), which showed with the finer resolutions of the TRMM 3B42 dataset that the diurnal peak of rainfall over Central America in the summer season is around 21:00 LST or later, while over the surrounding oceans, the gradients of the time of the diurnal rainfall peak are relatively larger (ranging from ~00:00 LST to 18:00 LST; Diro et al. 2012). Furthermore, diurnal variations explained nearly 70% of the daily variance during the boreal summer season over the region,

making this temporal scale key to studying Central American summer climatology. In addition, they indicate that the diurnal variation of precipitation in the boreal summer season is higher over Central America, with the oceans containing a fraction of the diurnal rainfall amplitude over land, except in the Gulf of Panama and along the coastal ocean of Colombia where it is comparable or even exceeds the terrestrial diurnal amplitude.

1.2 Oceanography of Central America

The warm eastern Pacific Ocean and the Caribbean Sea also serve as key climatic factors for Central America, a notable feature of the region being the Western Hemisphere Warm Pool (WHWP) (Wang and Enfield 2001; Amador et al. 2006, 2008). The WHWP is a pool of sea-surface temperatures at or exceeding 28.5 °C that, at its greatest extent, consists of portions of the eastern tropical North Pacific, Gulf of Mexico, Caribbean Sea, and western North Atlantic. The WHWP first develops in the eastern tropical North Pacific during the early boreal spring and gradually expands into the Intra-Americas Seas as the boreal summer begins and incoming shortwave flux, which fuels its growth, increases. This pool of warm SSTs is highly influential to the region's weather and climate, as it is generally associated with reduced static stability, sea-level pressure, and vertical wind shear, all necessary elements for the formation of organized tropical convection such as tropical easterly waves and tropical cyclones (Hidalgo et al. 2020).

In addition, surrounding ocean currents enable downwelling and upwelling, which are key to biological productivity and, by extension, the climate system. The Costa Rica Dome is a notable feature within this regional ocean current system, making its proper simulation a necessary piece of Central American climate analysis (Fielder 2002; Amador et al. 2006). The Costa Rica Dome is an annual shoaling of thermocline depths within the tropical eastern North Pacific, which first appears off the Costa Rican coast in late boreal winter and early boreal spring due to the wind stress imparted by the nearby Papagayo and Tehuantepec Low-Level Jets. Gradually, this area of shallow thermoclines, indicative of significant upwelling, expands and moves away from the coast, providing nutrient-rich water for various oceanic ecosystems.

1.3 Complexities of Simulation of Central American Climate

Due to the climate features mentioned previously, in combination with complex geography and various internal and external fluctuations such as ENSO, tropical North Atlantic SSTs (Misra

et al. 2014; Durán-Quesada et al. 2017, 2020), and periodic landfalling tropical cyclones, simulating the climate of Central America proves a daunting task (Alfaro et al. 2018; Misra and Jayasankar 2022 [hereafter, MJ22]; Kowal et al. 2023; Rodgers et al. 2024). General Circulation Models (GCMs) are a generally useful tool for climate simulation but struggle to model and project Central America's climate due to their relatively low resolution struggling with complex features such as local orographic interactions (Hidalgo et al. 2015; Almazroui et al. 2021; Baldwin et al. 2021). Therefore, as an alternative, higher resolution Regional Climate Models (RCMs) forced by some of these coarsely resolved GCMs at the lateral boundaries provide a viable strategy for simulating the climate over Central America (Cabos et al. 2019; Castro et al. 2018; Cavazos et al. 2020, Corrales-Suastegui et al. 2020, Torres-Alavez et al. 2021). However, prior studies were conducted by downscaling only the atmospheric component of a regional atmospheric model, with few using a coupled ocean-atmosphere model (e.g., Li and Misra 2014; Cabos et al. 2019; MJ22). From a practical standpoint, high-resolution earth system models that account for how the ocean and atmosphere coexist and evolve through the exchange of surface fluxes are preferred numerical tools for predicting or projecting a coupled climate system, especially in a geographic region such as Central America.

In this study, we are comparing the regional coupled ocean-atmosphere simulation in MJ22 with another simulation from an identical model setup, with the exception being the cumulus parameterization scheme in the atmospheric component of the RCM. Similar earlier intercomparison studies of convective parameterization schemes were conducted in the atmospheric model component, either using a single-column model (e.g., Xie et al. 2002) or the full atmospheric model (e.g., Martinez-Castro et al. 2018). The single-column model, as the name suggests, functions by using a grid column of an atmospheric model where the large-scale advective tendencies are specified from observation or large-scale models, and the model parameterizations are integrated forward in time. These tests provide a controlled setting that allows for understanding the specific behavior of a given cumulus parameterization scheme, but they operate under an idealized nature. A more realistic test would be to compare these parameterization schemes in earth system models where the parameterized convection interacts across spatio-temporal scales and with all climate system components, which this study aims to do. This study tests the cumulus parameterization scheme in a regional coupled ocean-atmosphere model over Central America, unlike previous studies conducted with only the regional atmospheric

model (e.g., Mapes et al. 2004; Martinez-Castro et al. 2018). Testing these cumulus parameterization schemes is vital, given the prominence of precipitating systems in the Central American region over the terrestrial and surrounding oceanic regions.

CHAPTER 2

DATA AND METHODS

2.1 Model Description

The model utilized in this study is the Regional Spectral Model-Regional Ocean Modeling System (RSM-ROMS), which is identical to that used in MJ22. RSM-ROMS is a regional, coupled ocean-atmosphere model that has been widely employed in regional climate modeling research spanning many domains around the globe (Li et al. 2014; Li and Misra 2014; Ham et al. 2016; Misra et al. 2018).

2.1.1 RSM Description

The atmospheric component of RSM-ROMS is RSM, which was introduced in Juang and Kanamitsu (1994). RSM utilizes the spectral method to calculate two-dimensional advective derivatives using sine and cosine functions with wall boundary conditions (Tatsumi 1986). Furthermore, RSM employs a semi-implicit time integration scheme and consists of 28 terrain-following sigma levels containing irregular vertical spacing, mirroring the National Centers for Environmental Prediction-Department of Energy (NCEP-DOE) Reanalysis (R2; Kanamitsu et al. 2002), with the top of the atmosphere at approximately 2 hPa. A scale-selective bias correction method, identical to that of Kanamitsu et al. (2010), is implemented to mitigate synoptic scale drift in integrating RSM. The width of the sponge zone surrounding the lateral boundaries is 16 grid points. The physics package utilized in RSM for this study is detailed in Table 1.

Table 1: Outline of RSM Physics Package

Physical process parameterized	Reference
Boundary layer	Hong and Pan (1996)
Prognostic clouds	Zhao and Carr (1997)
Gravity wave drag	Alpert et al. (1988)
Longwave radiation	Chou et al. (1996)
Shortwave radiation	Chou and Suarez (1994)
Land surface model	Ek et al. (2003)
Deep convection	Kain and Fritsch (1993)
InShallow convection	Tiedtke (1983)

2.1.2 RAS and KF2 Differences

The only difference between the versions of RSM-ROMS used in MJ22 and this study is that in the former the Relaxed Arakawa Schubert scheme (RAS; Moorthi and Suarez 1992) was used while the latter uses the Kain-Fritsch (KF2; Kain and Fritsch 1993; Kane 2004) cumulus parameterization. The fundamental differences between the two schemes are outlined in Table 2.

Table 2: Key Differences Between RAS and KF2 Schemes

Feature	RAS	KF2
Concept	Quasi-equilibrium theory: convection acts to maintain equilibrium between large-scale forcing and the cloud ensemble.	Mass flux scheme: focuses on triggering convection when certain criteria of instability and moisture availability are met.
Triggering of convection	No explicit triggering of convection. Convection is continuously active to relax instability over time.	Explicit convection triggering once a convectively available potential energy (CAPE) and moisture convergence threshold is reached.
Closure mechanism	Based on quasi-equilibrium theory.	Based on stabilizing the atmosphere by removing CAPE.
Adjustment	Gradual relaxation timescale of a half hour.	Rapid convection onset once triggering conditions are met.
Cloud representation	A spectrum of cloud types with different detrainment levels.	Single column convective cloud model, that explicitly calculates the mass flux and entrainment/detrainment of air between the convective updrafts/downdrafts and the surrounding environment

2.1.3 ROMS Description

ROMS is the oceanic component of RSM-ROMS similar to that used in Haidvogel et al. (2000) and Shchepetkin and McWilliams (2005). ROMS is a free surface, terrain-following primitive equation model, which uses a split explicit time-stepping scheme. To discretize the primitive equations in the vertical direction, ROMS utilizes stretched, terrain-following coordinates with 30 levels. In addition, ROMS incorporates several sub-grid scale parameterizations like the local closure schemes based on the level 2.5 turbulent kinetic energy equations developed by Mellor and Yamada (1982), the generic length-scale parameterization (Umlauf and Burchard 2003), the second-order biharmonic horizontal diffusion (Ezer et al. 2002), and the nonlocal closure scheme based on the K profile boundary layer formulation (Large et al. 1994) for surface and bottom oceanic boundary layers.

2.2 Experiment Design and Data

The atmospheric fluxes and SSTs exchange at a coupling interval of 1 hour between RSM-ROMS without using a flux coupler since they share identical grids. In addition, no flux corrections are applied during the integration. RSM-ROMS operates under a grid spacing of 15 km, simulating a domain identical to that seen in MJ22. For each simulation, the initial and lateral boundary conditions for the atmosphere are forced by the R2 reanalysis, and the lateral boundary conditions for RSM are updated every 6 hours (Kanamitsu et al. 2002). The ROMS ocean initial and lateral boundary conditions are forced by the Simple Ocean Data Assimilation version 2.4 (SODA; Carton and Giese, 2008). The temporal domain of the RSM-ROMS model output used in this study ranges from January 1, 1986, to December 31, 2001. Hereafter, the RSM-ROMS integration of this study will be referred to as RR-KF2 and that of MJ22 as RR-RAS. The datasets used to verify the RSM-ROMS output can be seen in Table 3. Model output biases for each variable are evaluated by computing them on the observational or reanalysis grid and are tested for significance using t-tests, with linear interpolation allowing for analysis between verification datasets of differing resolution from the models.

To directly compare the performance of the RSM-ROMS versions relative to observations, Taylor diagrams were incorporated into the analysis of several variables (Taylor and Karl 2001). Taylor diagrams are a method of statistical analysis in which model output can be evaluated by its standard deviation and pattern correlation coefficient simultaneously through a triangle inequality

relation between these measures. On Fig. 3, the x-axis and y-axis denote normalized standard deviations of the model output, which are proportional to the distance from the dashed unit circle, the unit circle representing the idealized standardized variance seen in observations. If the model output falls anywhere outside of the unit circle, the standard deviation will quantify the degree to which the model output misses the idealized variance. Furthermore, the arc denotes the pattern correlation coefficient, with higher correlation values near the bottom of the arc. The pattern correlation measures the degree to which the model output is in phase with observations. Ideally, the model output would have its standard deviation fall near or along the unit circle (labeled as REF for the figures of this paper) and along the bottom of the arc of the diagram, meaning the model accurately simulates the variability (or spatial gradients) and phase of a given variable seen in observations. It is worth noting that any variable analyzed in this study which did not incorporate a Taylor diagram was used as supporting material for the primary results; therefore, additional Taylor diagrams for those variables were not considered necessary.

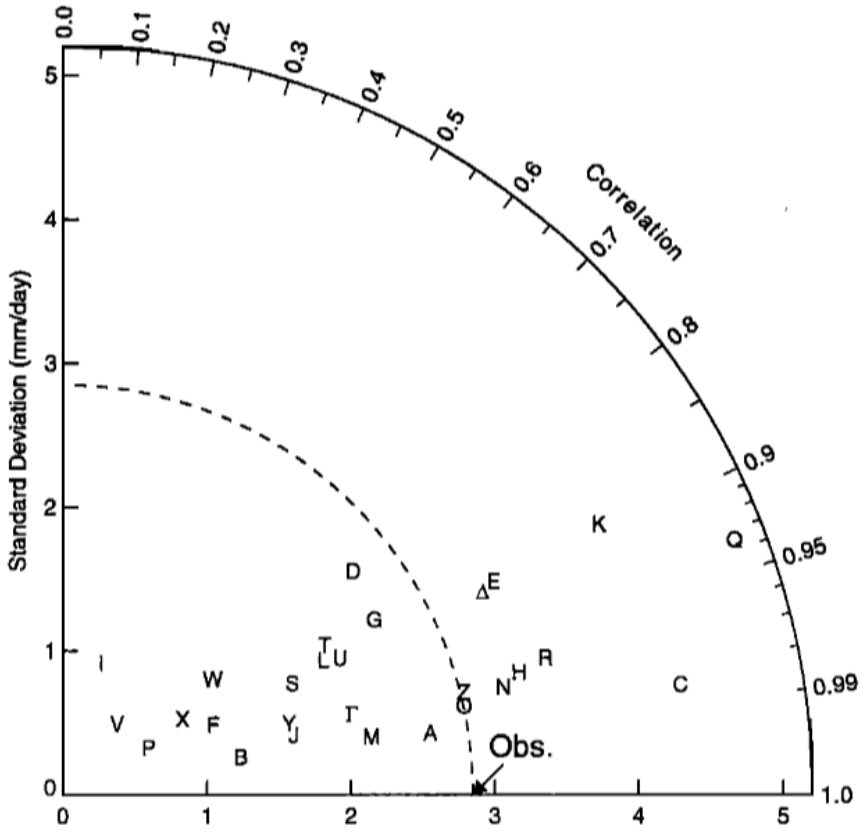

Figure 3: Example of Taylor Diagram in use, with the x and y axes denoting standardized variance and the arc denoting the pattern correlation. The unit circle is denoted with dashed lines. From Taylor (2001).

Table 3: Verification Datasets Used in the Study

Variable	Source	Purpose	Spatial resolution	Period used in the study
Rainfall	IMERG v7 (Huffmann et al. 2019)	Verification of seasonal mean surface precipitation, diurnal rainfall phase/amplitude, and MSD intensity/frequency	0.1° x 0.1°	2001-2023
SST	OISSTv2 (Reynolds et al. 2007)	Verification of seasonal mean sea-surface temperatures	0.1° x 0.1°	1986-2001
Depth of 20°C isotherm/surface ocean currents	SODA reanalysis (Carton and Giese 2008)	Verification of seasonal mean 20°C isotherm and surface ocean currents	1° x 1°	1986-2001
Enthalpy fluxes	OAFlux (Yu et al. 2008)	Verification of latent and sensible heat flux	1° x 1°	1986-2001
Upper air variables	ERA5 (Hersbach et al. 2019)	Verification of seasonal mean 850/925 hPa winds	0.5° x 0.5°	1986-2001

CHAPTER 3

RESULTS

3.1 Seasonal Climatology

3.1.1 Surface Rainfall and Convection Type

Fig. 4 displays the seasonal mean precipitation from model simulations, their comparison with corresponding observations, and direct comparison with each other. IMERG observational data outlines the expected seasonal climatology, where the highest surface precipitation occurs during the wet season (JJA and SON), which is mostly absent during the dry season (DJF and MAM) outside of coastal Colombia. Analysis of the model output reveals large, significant differences between the two simulations over the terrestrial and oceanic regions of the domain, one such difference being the reduction of the terrestrial wet bias of RR-RAS across all seasons in RR-KF2. Notable results also appear over the Caribbean, one example being the severe dry bias off the Caribbean coast of Costa Rica and Panama simulated by RR-RAS, which RR-KF2 subdues in all seasons. However, RR-KF2 does contain a prominent and persistent dry bias throughout the western Caribbean (Figs. 4i-l, 4q-t, and 4u-x). Over the eastern Pacific, both models simulate an erroneous northward displacement of the east Pacific ITCZ during the boreal summer and fall in the form of a dipole structure, with a northward wet bias along coastal Nicaragua and a southward dry bias. While RR-KF2 projects less northward surface rainfall than RR-RAS, RR-KF2 contains a worsened southward dry bias. The combination of reduced northward and southward precipitation within the ITCZ bias dipole suggests that RR-KF2 contains a weaker east Pacific ITCZ overall, further confirmed by RR-KF2 simulating drier surface conditions in both portions of the dipole when directly compared to RR-RAS (Figs. 4k-l, 4s-t, and 4w-x).

These qualitative observations are confirmed in the quantitative estimates shown as pattern correlations and standard deviation in the Taylor Diagram of Fig. 4y. RR-KF2 and RR-RAS perform similarly when all domain points or solely oceanic points are considered, reflecting their individual and shared biases. The greatest changes in model performance appear for terrestrial rainfall points, with RR-KF2 significantly improving upon the low pattern correlations and high standard deviation scores of RR-RAS, reflecting the reduction in the terrestrial wet bias seen in the former. Nonetheless, a problematic and significant terrestrial wet bias remains for RR-KF2, which is particularly evident in the boreal summer and fall, the time of the year coinciding with

the wet season of Central America and the MSD along the Central American Pacific slope (Magaña et al. 1999; Amador et al. 2006, 2008; Hidalgo et al. 2015; Sáenz et al. 2023). The relatively poor scores for standardized deviation and pattern correlation for land points indicate that terrestrial landfall is particularly challenging for RR-RAS, and to a lesser extent RR-KF2, to project accurately (Fig. 4y).

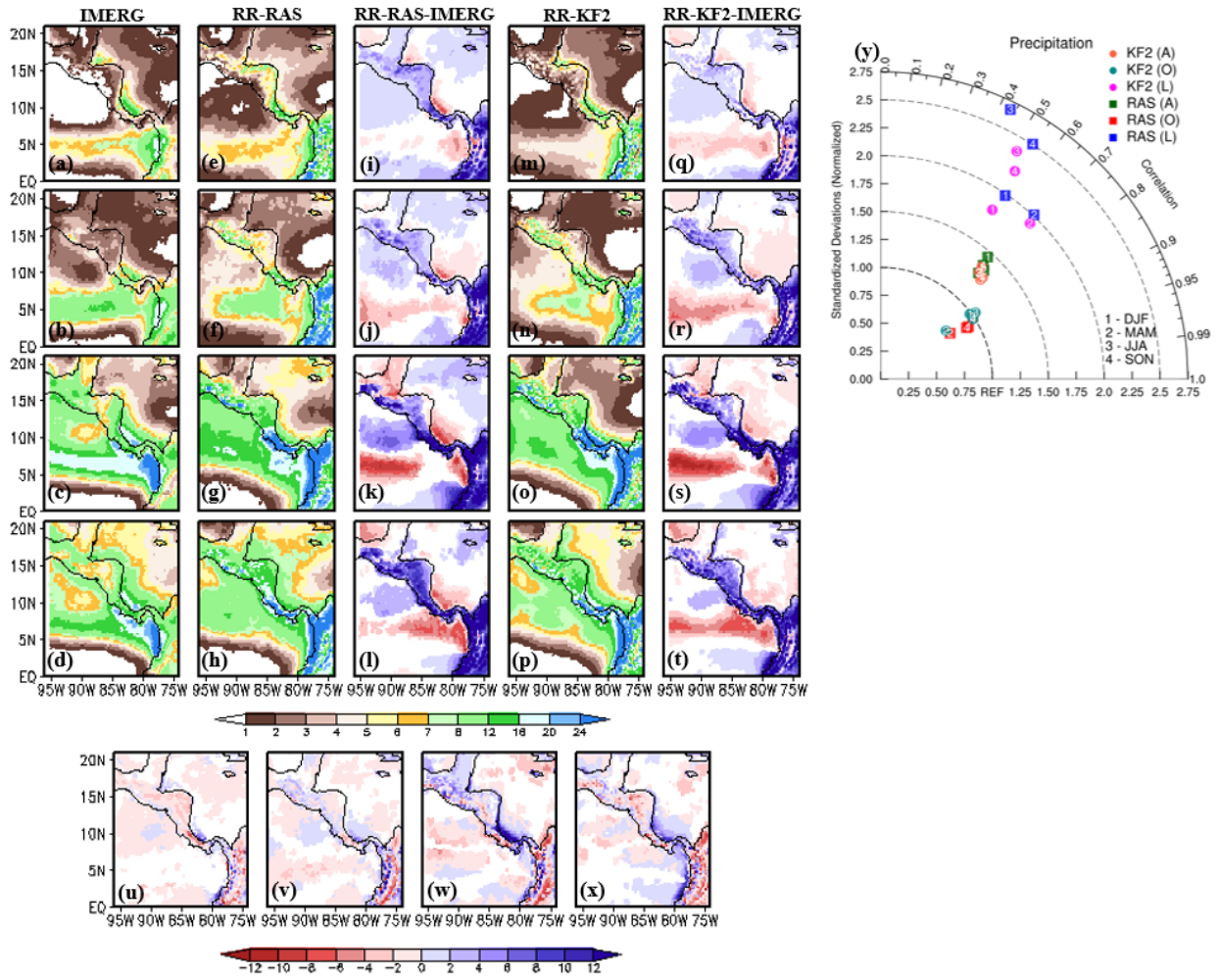

Figure 4: The seasonal mean climatological rainfall (mm day^{-1}; shaded) from (a, b, c, d) observations (IMERG) and (e, f, g, h) RR-RAS, (I, j, k, l) systematic errors of RR-RAS, (m, n, o, p) RR-KF2, (q, r, s, t) systematic errors of RR-KF2 and (u, v, w, x) difference of (RR-KF2) – (RR-RAS). The differences are shaded in (u, v, w, x) only if they exceed 95% confidence interval. In each column, the season order from top to bottom is DJF, MAM, JJA, and SON, with panels (u, v, w, and x) going from DJF on the far left to SON on the far right. (y) The values of the pattern correlation coefficient along the arc and the ratio of the standardized variances of the model to observations along the x-and y-axes are plotted in the Taylor diagram for all points (A), for all land points only (L) and for all ocean points only (O) in the domain.

Further analyzing the surface rainfall climatology can reveal whether the precipitation is more stratiform or convective, providing insight into the nature of the modeled convection and how each model behaves within the domain. The results of Figs. 5 and 6 indicate that RR-KF2 produces greater convective precipitation and less stratiform precipitation throughout the domain and in all seasons than RR-RAS. When viewing the results of Fig. 5, RR-KF2 produces the most convective rainfall over RR-RAS within the Central American landmass and along the coasts. These land types are commonly associated with short-lived and intense convective rainfall due to forcings such as sea breezes and land heating, which further influence thermodynamic parameters such as moisture convergence and CAPE (Alfaro 2002; Mapes et al. Part 1, Part 3 2003; Hidalgo et al. 2023). Recalling that terrestrial and coastal locations were areas where RR-KF2 improved upon RR-RAS in the surface rainfall climatology, it follows that the physics of RR-KF2 may provide a more accurate simulation of rainfall in terrestrial and coastal regions, where mesoscale and synoptic scale features interact with environmental parameters such as moisture convergence and CAPE, that then play a prominent role in convection initiation (Fig. 4 and Fig. 5i-l).

Conversely, when viewing the results of Fig. 6, there are distinct signatures of negative stratiform precipitation throughout the open oceans across all seasons, indicating that RR-RAS produces greater stratiform precipitation in these portions of the domain (Fig. 6i-1). Recalling that RR-KF2 contained dry biases over the east Pacific ITCZ and other portions of the open ocean, such as the western Caribbean Sea, there is an indication that RR-KF2 may struggle with convection tied to more oceanic environments (Figs. 4q-t and 4u-x). Tropical oceanic environments are associated with persistent regions of deep convection, in which stratiform rainfall forms through means such as the sustaining of the marine boundary layer and the approximately moist-adiabatic atmosphere (Emanuel 1994; Houze 1997; Schumacher and Houze 2003; Schumacher and Funk 2023). The deep convection that allows stratiform rainfall to occur in the oceanic tropics operates under a theoretical quasi-equilibrium structure, in which the environment continuously expends energy and forms convection to keep the atmosphere at a relatively constant state (Emanuel 1994). Therefore, the quasi-equilibrium physics of RR-RAS would produce more stratiform rainfall than RR-KF2, as it better matches the atmospheric dynamics within the tropical oceans (Fig. 6i-l). Another interesting result can be seen in panels Fig. 6k and 6l, in which there are notable signals of reduced stratiform precipitation by RR-KF2 within the east Pacific ITCZ and mountainous regions such as the continental divide. Houze (1997) notes that convective and

stratiform rainfall coexist within deep tropical convection, in which intense convective rainfall occurs within newer portions of the cumulonimbus cloud while calmer stratiform rainfall occurs within older portions. Cloud representation in RR-KF2 may miss the development of these complex cloud systems with varying ages and rain classifications, unlike RR-RAS, which contains multiple cloud and detrainment types (Table 2). Therefore, RR-KF2 lacks the stratiform rain occurring within deep convective areas created by large-scale convergence along the ITCZ and mountainous regions, exacerbating the previously mentioned dry biases of RR-KF2 and further displaying the nuance in the simulated surface rainfall climatology, possibly containing implications for the simulation of other climate parameters.

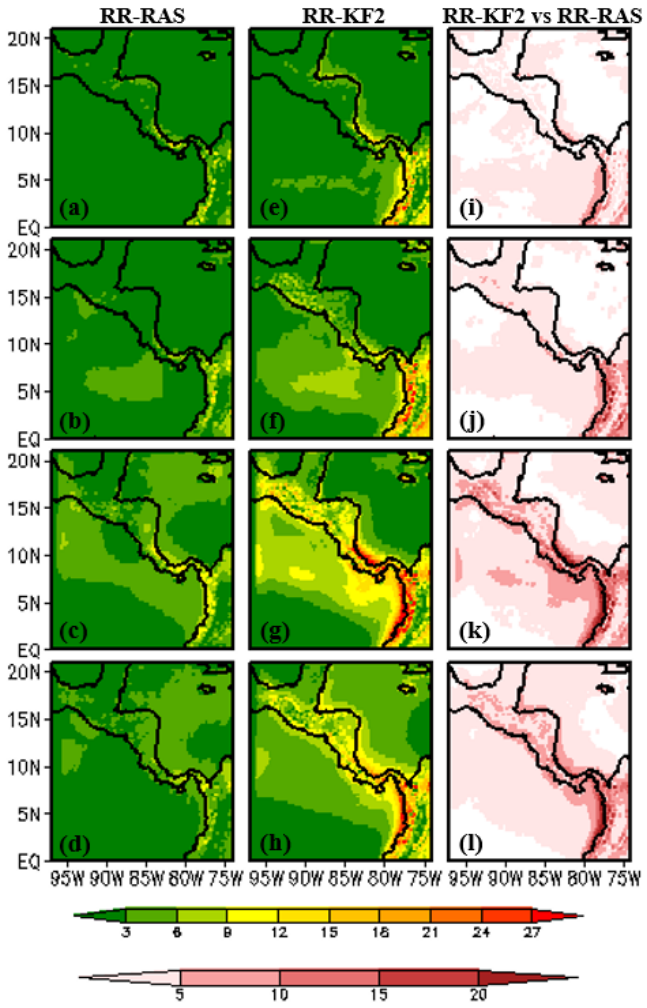

Figure 5: The seasonal mean climatological convective precipitation (mm/day; shaded) from (a, b, c, d) RR-RAS and (e, f, g, h) RR-KF2, and (i, j, k, l) difference of (RR-KF2) – (RR-RAS). The differences are shaded in (i, j, k, l) only if they exceed 95% confidence interval.

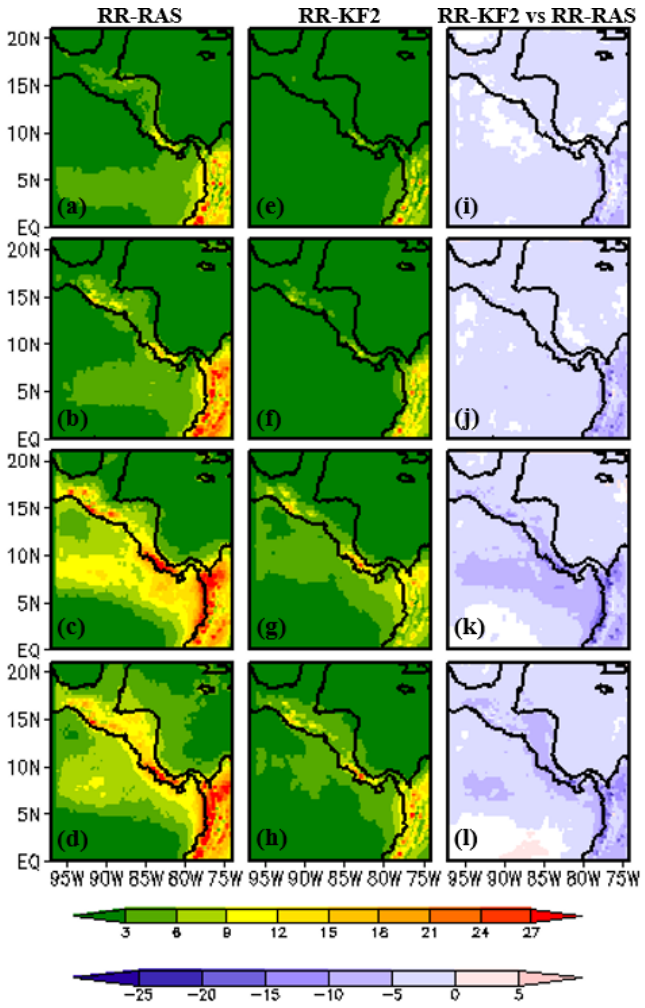

Figure 6: The seasonal mean climatological stratiform precipitation (mm/day; shaded) from (a, b, c, d) RR-RAS and (e, f, g, h) RR-KF2, and (i, j, k, l) difference of (RR-KF2) – (RR-RAS). The differences are shaded in (i, j, k, l) only if they exceed 95% confidence interval.

3.1.2 Precipitable Water

The comparisons of the model simulations for seasonal mean precipitable water are shown in Fig. 7. ERA5 parallels the seasonal surface rainfall climatology of Fig. 4, in which the highest precipitable water is restricted to Coastal Colombia during the dry season, followed by an expansion of moist air columns into the Central American landmass and beyond during the wet season (Figs. 7a-d). The model biases in precipitable water are comparable in RR-RAS and RR-KF2 across all seasons, both models containing a land wet bias for the boreal winter and spring and an oceanic dry bias during the boreal summer and fall (Figs. 7i-l and 7q-t). However, the oceanic dry bias is marginally relieved in RR-KF2 relative to RR-RAS, particularly in the east

Pacific (Figs. 7u-x). The corresponding Taylor Diagram in Fig. 7y for precipitable water, unlike in Fig. 4y for precipitation, shows both models with standard deviation scores less than one across the domain, suggesting weaker spatial gradients in the model simulations compared to ERA5. This statistical finding aligns with both models lacking precipitable water over the Colombian coast and ITCZ region, leading to weaker spatial gradients (Figs. 7g-h and 7o-p). Furthermore, similar to Fig. 4y, land points remain a point of contention in the simulations with lower pattern correlations compared to the domain when solely oceanic points or all domain points are considered (Fig. 7y).

The results of Figs. 4 and 7 suggest that the simulation of seasonal rainfall and its associated moisture content are aspects of Central American climate simulation that will need significant future enhancements, particularly over land. In terms of the possible causes behind these respective biases, previous literature may provide insight. Duran-Quesada et al. (2017) note that the primary moisture source for the subdued convection of the Central American dry season is local moisture recycling through the evapotranspiration of local rainforests (Duran-Quesada et al. 2017). Despite the absence of large-scale forcings such as the ITCZ during the dry season, RR-RAS, and to a lesser extent RR-KF2, still produce a notable terrestrial wet bias for surface rainfall and atmospheric moisture. One possible reason behind these terrestrial biases may be an excess of moisture advection or recycling over land, leading to an erroneously moist atmospheric column and meeting of the convection thresholds, leading to abnormally high surface rainfall. For RR-RAS, erroneously high moisture content would lead to a frequent loss of the quasi-equilibrium state, leading to convection initiation to return to said state. Conversely, for RR-KF2, moisture convergence and CAPE thresholds would be reached enough to create excessive convection and surface rainfall. However, this theory does not fully explain why, in summer and fall, the wet bias for the surface rainfall remains, but the bias in the precipitable water switches to a dry bias. This dilemma opens a second possible explanation, that being the interactions RR-RAS and RR-KF2 have with the local topography. Throughout the dry and wet seasons, the highest bias signatures in both models coincide with the mountainous terrain of the continental divide (Figs. 4i-l, 4q-t, 7i-l, and 7q-t), these biases also coincide with areas of elevated convective and stratiform rainfall (Figs. 5 and 6). It is likely that as the convection thresholds of these models interact with topography through processes such as orographic lift, excessive rainfall occurs, indicating heightened sensitivity to topographic interactions. This relationship would explain why a precipitable water dry bias and surface rainfall wet bias could exist over the landmass during the wet season since

multiple short rain bursts would lead to high surface rainfall and dry the atmospheric column. Further investigation of how these models interact with local topography and moisture sources will be needed to determine the exact reason behind these biases, displaying another facet of the sensitivity regional climate simulations contain to changes to cumulus parameterization.

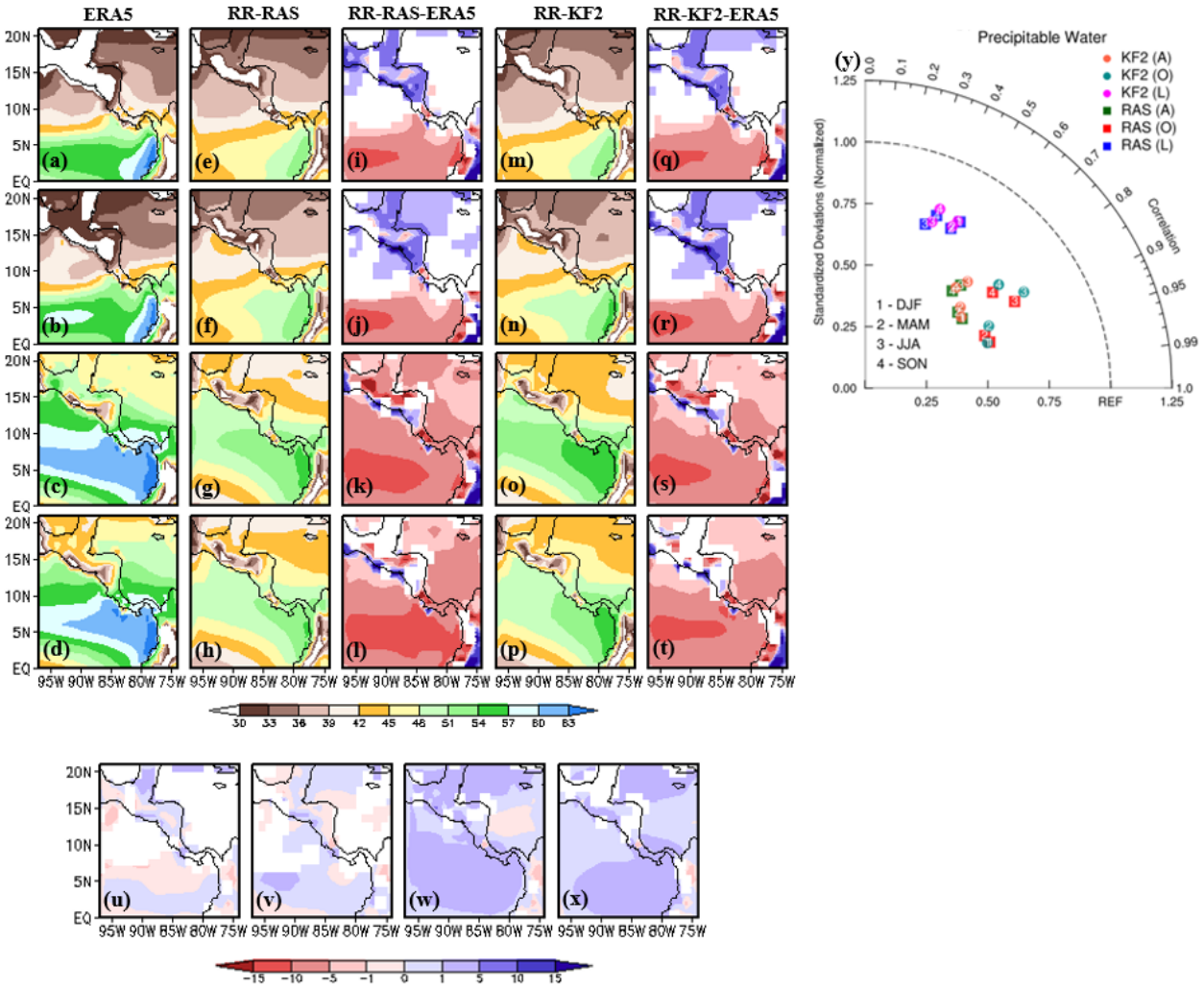

Figure 7: The seasonal mean precipitable water (kg m^{-2}; shaded) from (a, b, c, d) observations (NVAP) and (e, f, g, h) RR-RAS, (I, j, k, l) systematic errors of RR-RAS, (m, n, o, p) RR-KF2, (q, r, s, t) systematic errors of RR-KF2 and (u, v, w, x) difference of (RR-KF2) – (RR-RAS). The differences are shaded in (u, v, w, x) only if they exceed 95% confidence interval. (y)The values of the pattern correlation coefficient along the arc and the ratio of the standardized variances of the model to observations along the x-and y-axes are plotted in the Taylor diagram for all points (A), for all land points only (L) and for all ocean points only (O) in the domain.

3.1.3 850 hPa and 925 hPa Wind Field

To provide clarity into how these cumulus parameterization schemes affect wind field simulations of this region, the seasonal mean 850hPa winds are analyzed in Fig. 8. It is worth noting that while these LLJs contain their cores at 925 hPa, they have also been identifiable at 850 hPa, making 850 hPa an adequate pressure level for analysis (Mora 2017; Yepes et al. 2019). Regarding the CLLJ, at this pressure level, the westerly bias of RR-RAS over the Caribbean Sea is reduced in RR-KF2, indicated by the higher easterly wind signature in the Caribbean Sea during DJF and JJA (Figs. 8u and 8w). Therefore, RR-KF2 provides improvements in simulating the magnitude of the CLLJ, albeit at a weaker state than ERA5 (Figs. 8q-t). RR-KF2 simultaneously exacerbates the 850 hPa westerly wind bias in the eastern Pacific compared to RR-RAS, producing a weaker PaLLJ (Figs. 8u-v). Furthermore, concerning the PJ and TeLLJ, both models similarly replicate their respective annual maxima and geographic location by displaying a strong wind region within the Gulf of Panama and Isthmus of Tehuantepec during the winter and spring (Figs. 8e-f and 8m-n). The Taylor Diagram computed over all grid points in the domain in Fig. 8y shows that the zonal winds have higher pattern correlations in both model simulations than the meridional winds in the summer and fall seasons, which would lead to inaccuracies in more meridionally-oriented jets active during these seasons such as the CJ. Beyond this discrepancy, the pattern correlation and standardized variance skill for both models are generally comparable across all seasons for the 850 hPa winds (Fig. 8y).

At the 850 hPa pressure level, the signal of the CJ is too weak to discern in ERA5 and compare with RR-RAS and RR-KF2. Therefore, additional analysis was performed on the 925 hPa wind field to evaluate the model performance of the CJ while also providing analysis of the other LLJs at the pressure level of their cores (Davis et al. 1997; Poveda and Mesa 2000; Amador et al. 2006, 2008; Muñoz et al. 2008; Durán-Quesada et al. 2017; Hidalgo et al. 2015; Sáenz et al. 2023). The Choco Jet is visible in the westerly flow of Fig. 9d, which aligns with its most prominent period of October and November (Poveda and Mesa 2000). Evaluation of RR-RAS and RR-KF2 reveals an improved CJ simulation in the latter, albeit marginally stronger than ERA5 (Figs. 9t and 9u-x). Overall, the stronger simulation of the CJ in RR-KF2 is a key improvement in the wind field simulation, since the CJ provides a vital moisture belt to the Pacific coast during the fall (Poveda and Mesa 2000; Durán-Quesada et al. 2017).

Interesting results appear regarding the cores of the other regional LLJs, in which RR-RAS and RR-KF2 similarly place several LLJs too far to the west compared to ERA5, including TeLLJ, PJ, and CLLJ. Furthermore, the winds of the PaLLJ spread further north than ERA5, resulting in a less consolidated core region within Nicaragua and Costa Rica (Figs. 9i-l and 9q-t). Altering the cumulus parameterization scheme also alleviated or worsened biases concerning the wind magnitudes of these LLJ cores. In the boreal winter and spring, RR-KF2 reduces the strong PJ bias of RR-RAS but also produces an excessively strong TeLLJ. RR-KF2 does move the winter maxima of the CLLJ away from the western Caribbean but largely fails to do so for the summer maxima. For the PaLLJ, usage of RR-KF2 does not yield any significant improvements since it still places the jet core in the same location as RR-RAS (Figs. 9u-x).

A notable connection between variables appears when considering where the ITCZ is placed in the 925 hPa climatology of RR-RAS and RR-KF2. In ERA5, an axis of converging winds associated with the ITCZ can be seen south of 10 °N (Figs. 9c and 9d). Conversely, RR-RAS and RR-KF2 place this axis at 10 °N, suggesting a northward push of the ITCZ (Figs. 9g-h and 9o-p). This bias is further confirmed when viewing the RR-RAS and RR-KF2 observational biases in which both models place a notable southwesterly wind bias along the same latitude as the ITCZ in ERA5, pushing this feature northeast toward the landmass (Figs. 9k-l and 9s-t). Furthermore, the ITCZ axis of both models coincides geographically with the previously mentioned wet bias along the Pacific coast of Nicaragua, suggesting that changes to the wind field caused by the simulated convection impact synoptic-scale forcings such as the ITCZ, which could further influence surface precipitation (Figs. 4k-l and 4s-t). For instance, since the ITCZ axis of RR-RAS and RR-KF2 is closer to the landmass during the summer and fall, the convection brought by the ITCZ could exacerbate the terrestrial wet bias of those seasons. Therefore, it is key to investigate these ITCZ biases since the ITCZ is an influential feature for moisture advection and rainfall for the entire domain, in addition to other climatological variables.

The combined results of Figs. 8 and 9 imply that while RR-KF2 does provide improvements in the simulation of the wind climatology, there is room for improvement in the geographical placements of these jets and their structure, as several jets are projected as weaker or stronger at different pressure levels compared to ERA5. As previous and subsequent results show, how the wind field is modeled carries a series of cascading effects since much of Central American

climatology is controlled by the seasonal variations in the trade winds and their interaction with terrestrial and oceanic locations (Amador et al. 2006, 2008; Hidalgo et al. 2015; Sáenz et al. 2023). Therefore, it is vital to understand why RR-KF2 and other cumulus parameterization schemes generate their respective wind biases through convection initiation and how we can resolve them to better project the regional climate, enhancing the simulation of other climate parameters.

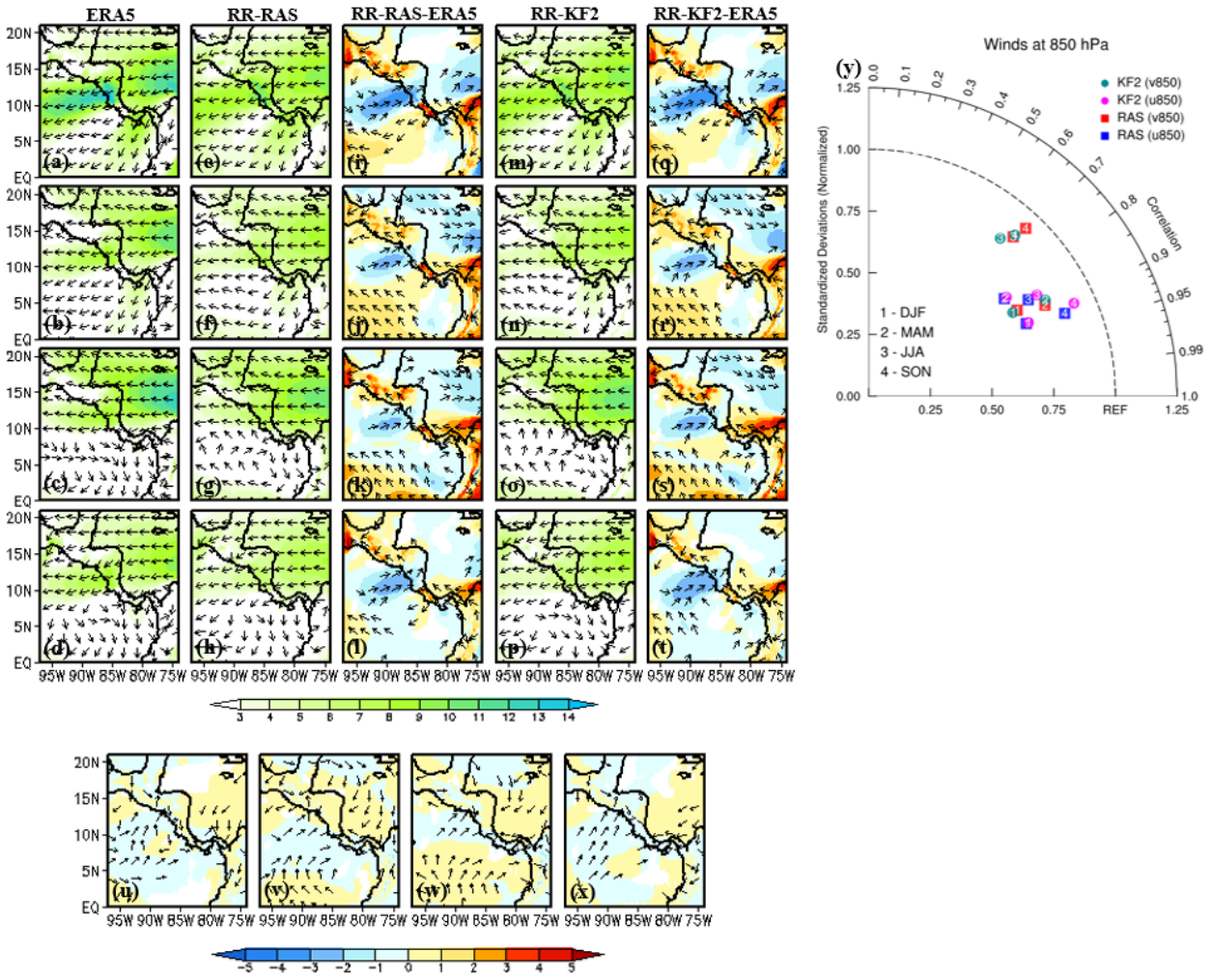

Figure 8: The seasonal mean 850 hPa winds (m s^{-1}) from (a, b, c, d) observations (ERA5) and (e, f, g, h) RR-RAS, (I, j, k, l) systematic errors of RR-RAS, (m, n, o, p) RR-KF2, (q, r, s, t) systematic errors of RR-KF2 and (u, v, w, x) difference of (RR-KF2) – (RR-RAS). The vectors are shown in (u, v, w, x) only if they exceed 95% confidence interval. (y) The values of the pattern correlation coefficient along the arc and the ratio of the standardized variances of the model to observations along the x-and y-axes are plotted in the Taylor Diagram for all points in the domain.

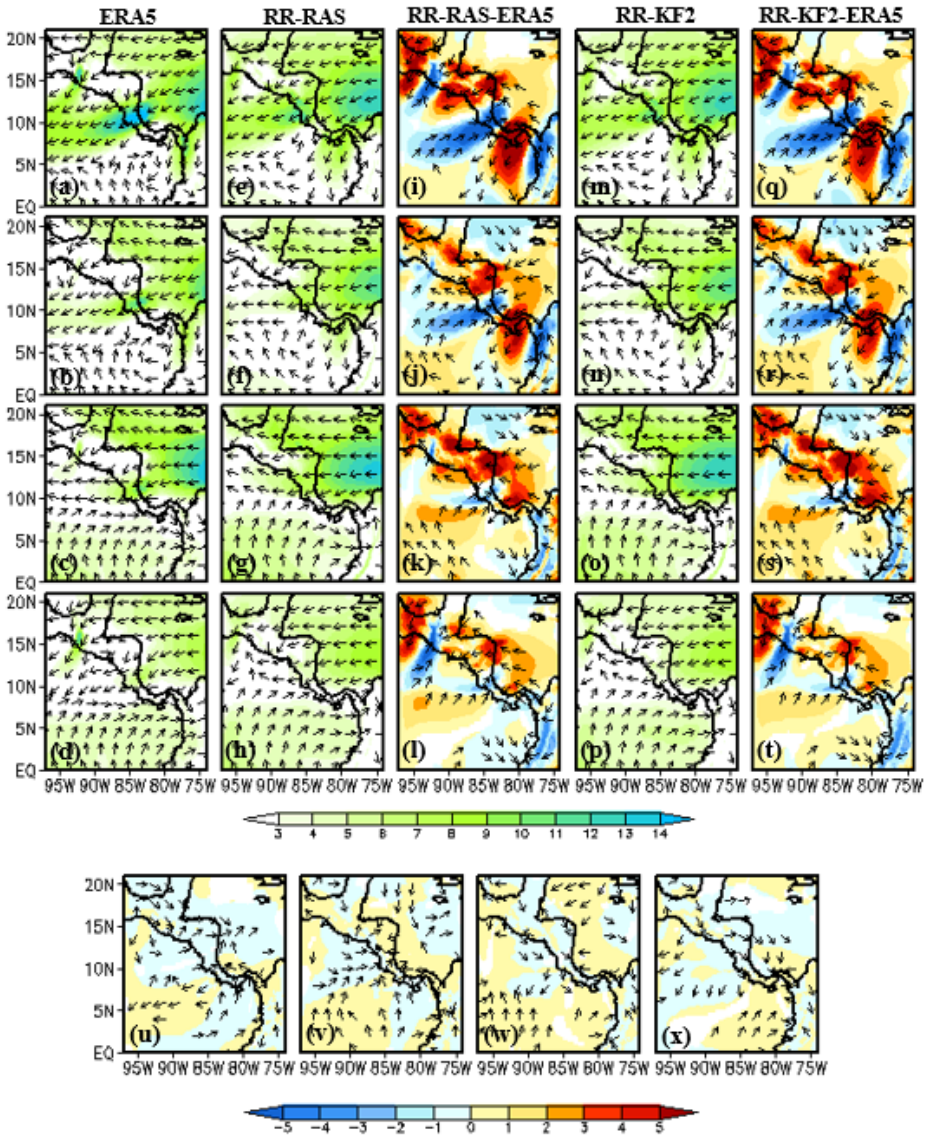

Figure 9: The seasonal mean 925 hPa winds (m s^{-1}) from (a, b, c, d) observations (ERA5) and (e, f, g, h) RR-RAS, (I, j, k, l) systematic errors of RR-RAS, (m, n, o, p) RR-KF2, (q, r, s, t) systematic errors of RR-KF2 and (u, v, w, x) difference of (RR-KF2) – (RR-RAS). The vectors are shown in (u, v, w, x) only if they exceed 95% confidence interval.

3.1.4 Sea-Surface Temperature (SST)

The seasonally averaged SSTs from OISSTv2 demonstrate the seasonal evolution of the WHWP from the pool forming in the east Pacific during the spring to its expansion into the Caribbean Sea during the summer and fall (Figs. 10a-d). RR-KF2 provides significant improvements in replicating this seasonal cycle compared to RR-RAS. For instance, the persistent

cold SST biases in the Gulf of Panama, the Venezuelan Coast, and the Pacific coast of Central America in RR-RAS during all seasons are significantly alleviated in RR-KF2 (Figs 10i-l and 10q-t). However, RR-KF2 contains a notable warm bias in the open waters of the Caribbean Sea and eastern Pacific. Particularly problematic areas for the RR-KF2 warm bias include the western Caribbean Sea during the spring and the cold tongue of the east Pacific during the summer and fall (Figs. 10r-t). The Taylor Diagram computed over all ocean grid points in the domain in Fig. 10y shows modest improvement in pattern correlations and substantial improvement in standard deviation for winter and spring in RR-KF2. This change is possible by reducing the widespread cold SST biases of RR-RAS, leading RR-KF2 to produce spatial gradients closer to observations. RR-KF2 and RR-RAS contain similar standard deviation and pattern correlation scores for the summer and fall, reflecting their ability to effectively simulate the intensity of the seasonal SST gradient despite their SST value biases (Fig. 10y).

Convection over the ocean and its clouds can potentially impart cloud radiative effects on the ocean surface, establishing a connection between the modeled convection and the SST simulation. For instance, low-level clouds may impart a surface cooling effect where the energy transfer from the ocean surface to the atmosphere needed to sustain convection allows SSTs to cool (Wang and Enfield 2001; L'Ecuyer et al. 2019). If convection is present enough, it could block incoming shortwave radiation from reaching the surface, allowing for additional SST cooling. However, a warming effect is also possible, in which cloud decks act to trap outgoing longwave radiation, enabling further warming. Unlike low-level clouds, high-level clouds are primarily associated with a surface warming effect, as they play a notable role in trapping outgoing longwave radiation (L'Ecuyer et al. 2019). Wang and Enfield (2001) emphasized the importance of SSTs and cloud radiative feedbacks for the annual development of the WHWP, in which they proposed a growth mechanism involving convection initiated by warm SSTs trapping longwave radiation and allowing SSTs to warm further. Magaña et al. (1999) also noted the key role SSTs and cloud radiative feedbacks in the WHWP played in initiating the Mid-Summer Drought. In this feedback, convection would block enough shortwave radiation to cool SSTs and enable the strengthening of easterly trade winds necessary for the Mid-Summer Drought to form. Therefore, it is imperative to analyze how RR-RAS and RR-KF2 simulate cloud cover in the lower and upper levels to investigate potential radiative feedbacks that would influence the SST stimulation.

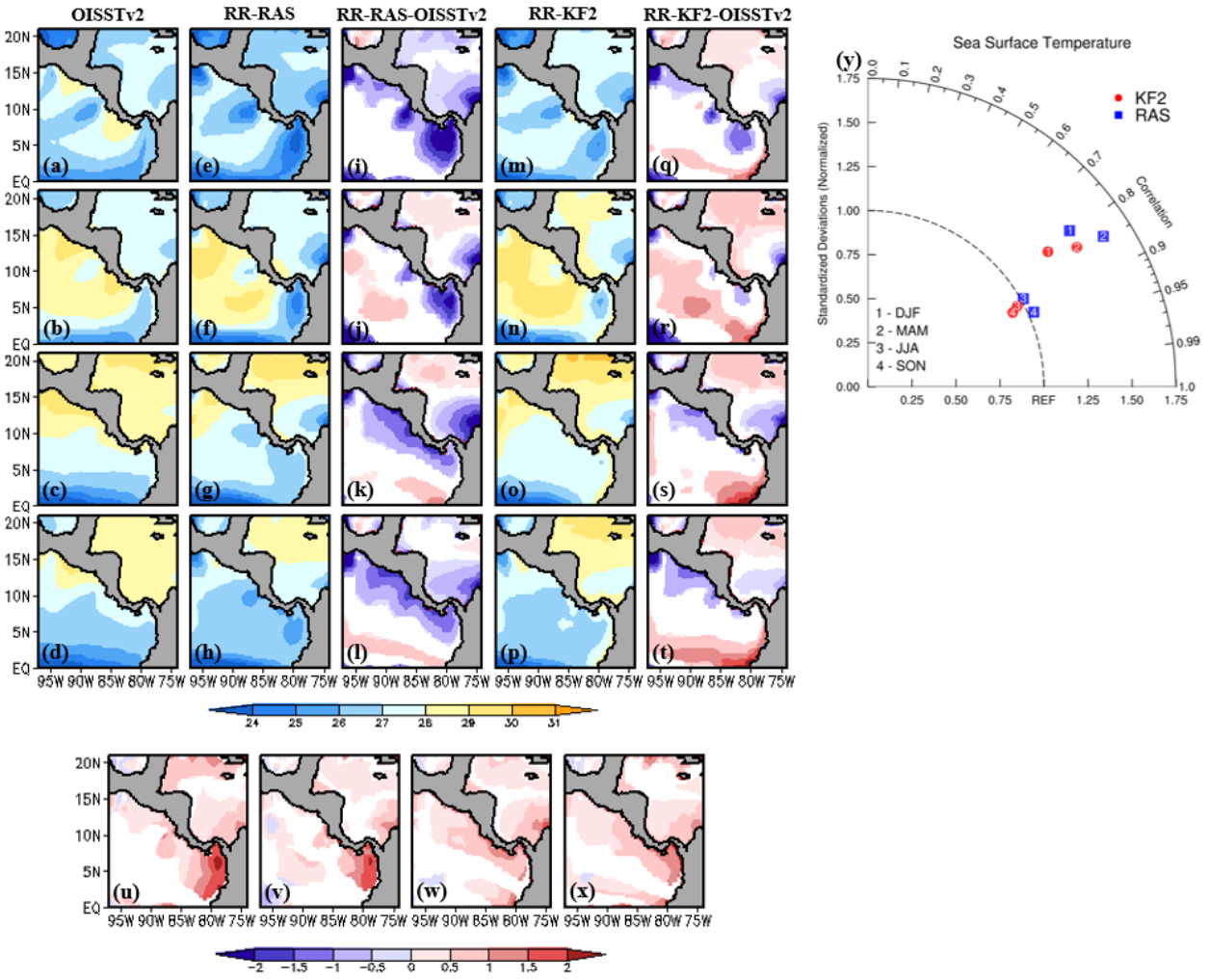

Figure 10: The seasonal mean climatological SST (°C; shaded) from (a, b, c, d) observations (OISSTv2) and (e, f, g, h) RR-RAS, (I, j, k, l) systematic errors of RR-RAS, (m, n, o, p) RR-KF2, (q, r, s, t) systematic errors of RR-KF2 and (u, v, w, x) difference of (RR-KF2) – (RR-RAS). The differences in (u, v, w, x) are shaded only if they exceed 95% confidence interval. (y) The values of the pattern correlation coefficient along the arc and the ratio of the standardized variances of the model to observations along the x-and y-axes are plotted in the Taylor Diagram for all points in the domain.

3.1.5 Cloud Cover

RR-KF2 produces an opposing response in the low-level and upper-level cloud cover of Figures 11 and 12, in which RR-KF2 produces less low-level cloud cover and more upper-level cloud cover than RR-RAS across all seasons (Figs. 11i-l and 12i-l). Mid-level cloud cover differences between the models were minor; therefore, they were not included in this analysis.

Reduced cloud cover at the low levels would allow increased shortwave radiation to reach the surface, supporting warming at the ocean surface. The bolstered upper-level cloud cover would then reinforce the surface warming feedback by trapping outgoing longwave radiation. While it is challenging to pinpoint the exact radiative feedback occurring in the models for the low-level clouds, these trends in cloud cover suggest the convection of RR-KF2 could support a warmer surface environment over oceanic and terrestrial points. Further supporting this point is that these cloud cover trends coincide with areas where RR-KF2 reduced the cold SST biases of RR-RAS, such as the Pacific coast of Central America and the Gulf of Panama (Fig. 10). However, it is important to note that wind-driven oceanic mixing may also play a role in the warmer SSTs of RR-KF2, making further analysis of the oceanic climatology necessary.

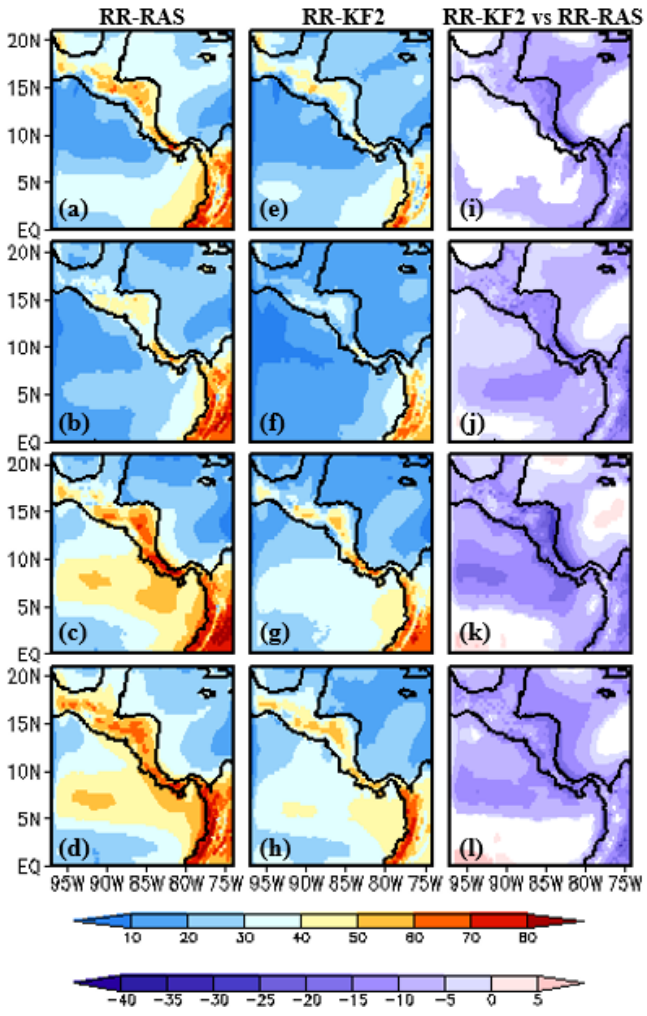

Figure 11: The seasonal mean climatological low-level cloud cover (%; shaded) from (a, b, c, d) RR-RAS and (e, f, g, h) RR-KF2, and (i, j, k, l) difference of (RR-KF2) – (RR-RAS). The differences are shaded in (i, j, k, l) only if they exceed 95% confidence interval.

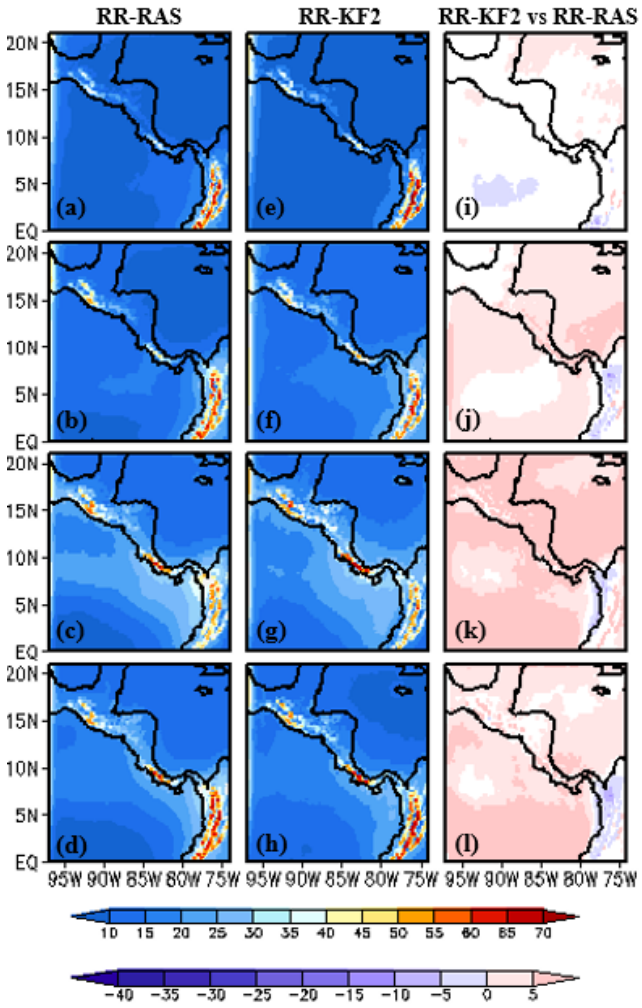

Figure 12: The seasonal mean climatological upper-level cloud cover (%; shaded) from (a, b, c, d) RR-RAS and (e, f, g, h) RR-KF2, and (i, j, k, l) difference of (RR-KF2) – (RR-RAS). The differences are shaded in (i, j, k, l) only if they exceed 95% confidence interval.

3.1.6 Thermocline Depth and Surface Ocean Currents

As the thermocline depths of Fig. 13 reveal, upper-ocean stratification in both models is weak, indicating a lack of mixing in the simulations (Fig. 13). The depth of the thermocline, as diagnosed from the depth of the 20°C isotherm, is shallow in both simulations of RSM-ROMS, although this bias is much weaker in the east Pacific compared to the Caribbean Sea. RR-KF2 does, however, make significant progress in reducing the shallow thermocline depth bias in both oceans relative to RR-RAS (Figs. 13u-x). The corresponding Taylor Diagram covering thermocline depth in Fig. 13y shows a significant quantitative improvement in pattern correlations

and standard deviation in RR-KF2 over RR-RAS, which is possible by producing deeper thermoclines in both ocean basins. This reduction of the shallow thermocline bias is likely tied to the warmer SSTs simulated by RR-KF2 since deeper thermoclines suggest improved mixing, which allows SSTs to remain warm. The ocean mixing enabling these improvements is controlled by the surface wind field imparting a wind stress on the ocean surface, which is influenced by the convection simulated in each model. Therefore, not only is the convection itself important when considering the impact of these cumulus parameterization schemes, but also the influence of their indirect effects, such as that on the wind field (Figs. 8, 9, 10, and 13). While it is difficult to decipher whether changes to oceanic mixing or cloud radiative feedbacks are more influential in the warming of SSTs in RR-KF2, both factors likely play a role in improving the SST simulation.

Despite the higher thermocline depths within a portion of the Pacific coast of Central America in RR-KF2, both models similarly underperform in the seasonal migration of the Costa Rica Dome. Both simulations of RSM-ROMS start adequately in the winter and spring, with the TeLLJ and PaLLJ enabling thermocline shoaling along the Pacific coast of Central America (Fielder 2002). As the ITCZ propagates north in the summer and fall and the LLJs wane in their influence, both models fail to separate the Costa Rica Dome from the coast (Figs. 13e-h and 13m-p). Struggles to properly simulate the seasonal migration of the Costa Rica Dome during this period likely relate to biases concerning ITCZ simulation in both models. Since RR-RAS and RR-KF2 place the ITCZ too far north and toward coastal Central America, the upwelling initiated by the ITCZ suffers the same issue, leading to thermocline depths that cling to the Pacific coast rather than coalescing closer to the equator (Figs 9 and 13).

In terms of the surface ocean currents, the south equatorial current is underestimated in both models, exemplified by a lack of northeasterly surface ocean currents near the equator in the boreal winter and spring, which is worsened in RR-KF2 (Figs. 13e-f and 13m-n). RR-KF2 and RR-RAS also struggle with surface current biases related to the wind stress imparted by the ITCZ in the summer and fall, with both model versions failing to produce the clockwise circulation seen in SODA within 90-80W and 0-5N, relating to their previously mentioned bias related to the ITCZ (Figs. 13c-d, 13g-h, and 13o-p). In the Caribbean, RR-RAS and RR-KF2 simulate erroneously easterly to northeasterly surface ocean currents across all seasons, which overlaps with the shallow thermocline depth bias near the coasts of Costa Rica and Panama (Figs. 13i-l and 13q-t).

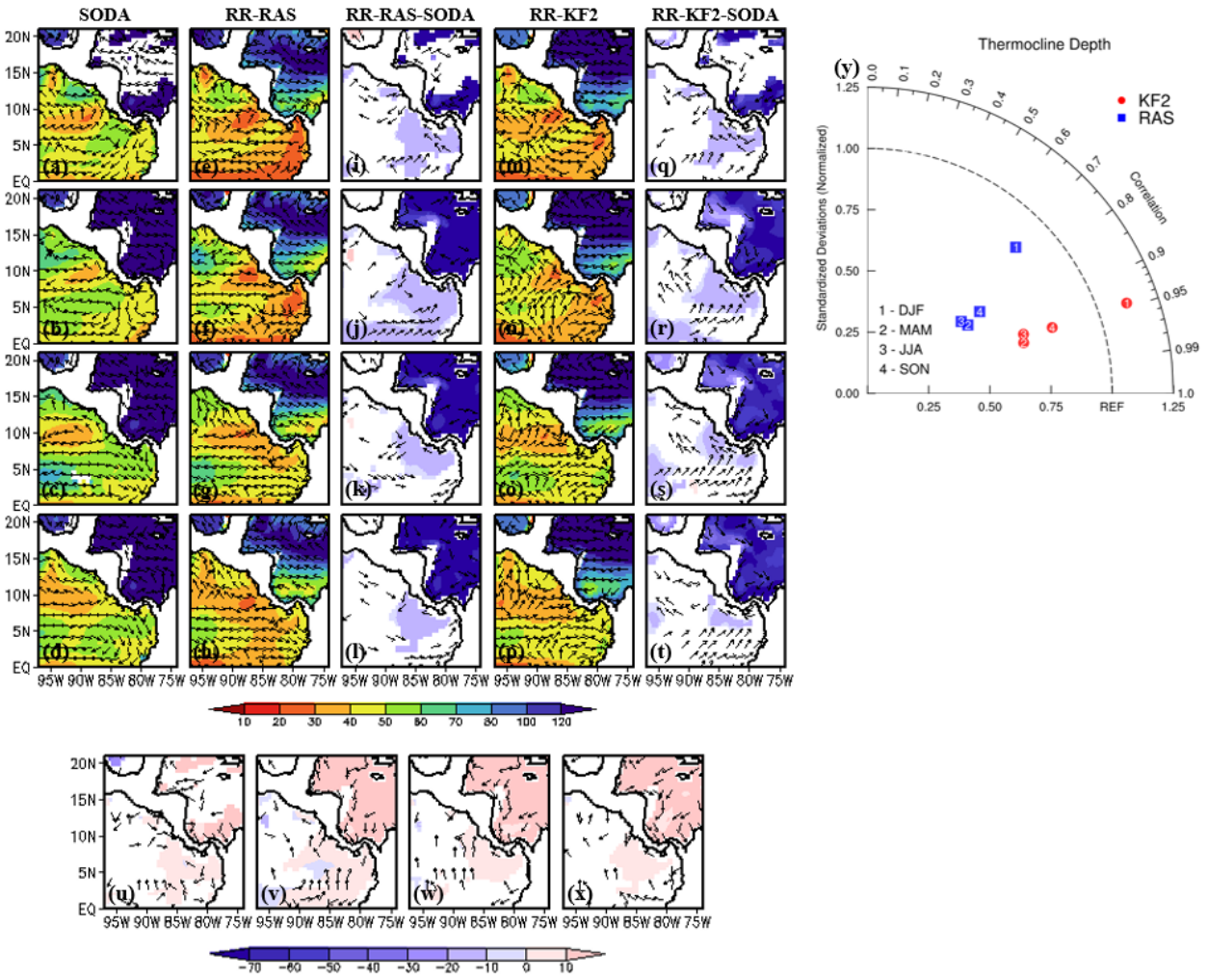

Figure 13: The seasonal mean climatological thermocline depth (m; shaded) overlaid with surface ocean currents from (a, b, c, d) observations (SODA) and (e, f, g, h) RR-RAS, (I, j, k, l) systematic errors of RR-RAS, (m, n, o, p) RR-KF2, (q, r, s, t) systematic errors of RR-KF2 and (u, v, w, x) difference of (RR-KF2) – (RR-RAS). The differences of the thermocline depth are shaded and surface currents (vectors) are shown in (u, v, w, x) only if they exceed 95% confidence interval. (y) The values of the pattern correlation coefficient along the arc and the ratio of the standardized variances of the model to observations along the x-and y-axes are plotted in the Taylor diagram.

3.1.7 Latent and Sensible Heat Fluxes

Before delving into changes appearing in other oceanic features, such as the latent heat flux values of Fig. 14, it is worth noting that in OAFlux, positive surface heat flux values (latent or sensible) indicate heat leaving the ocean surface and entering the atmosphere. The comparisons of the latent heat flux over the oceans in Fig. 14 indicate that RR-KF2 generates more latent heat flux than RR-RAS in all seasons, exemplified by the absence of negative latent heat flux values in the

RR-KF2/RR-RAS comparison (Fig. 14u-x). Generally, the SST and surface latent heat flux results coincide well, which is consistent with the general concept of warmer SSTs enabling greater latent heat flux if adequately strong winds are present. Therefore, since RR-KF2 warms SSTs across the board, it also uniformly increases the surface latent heat flux (Figs. 10 and 14). One area of significant improvement is the Gulf of Panama, in which RR-RAS greatly underestimates the latent heat flux during these seasons, likely due to the cold SSTs simulated there. These SSTs are significantly warmer in RR-KF2, allowing for greater latent heat flux as a result (Figs. 10e, 10m, 14e, and 14m). Other latent heat flux changes brought by the warmer SSTs of RR-KF2 can be seen in the Pacific Coast of Central America in the summer and fall and the Venezuelan coast year-round (Figs. 14i-l and 14q-t). Further reinforcing the sensitivity of the latent heat flux simulation to the SST simulation is that RR-KF2 also carries over the erroneous biases from its seasonal SST simulation. Most notable among these is the positive latent heat flux bias over the eastern Pacific cold tongue, coinciding with the warm SST bias RR-KF2 contains in the fall.

The negative or reduced sensible heat flux in Fig. 15 seemingly coincides with regions and seasons where LLJs are active. In the winter and spring, OAFlux displays a clear signal of negative or reduced sensible heat flux over the CLLJ, PaLLJ, and PJ, with negative sensible heat fluxes also visible during the secondary summer peak of the CLLJ (Figs. 8, 9, and 15). RR-RAS and RR-KF2 adequately replicate this spatial pattern, although both models underestimate the amount of sensible heat in the locations of the CLLJ and PJ (Figs. 15i-k and 15q-s). RR-KF2 does, however, improve upon the weak and strong sensible heat flux biases seen in RR-RAS, with varying sensible heat flux generated in coastal and open oceans to better match the climatology of OAFlux (Figs. 15u-x). It is worth noting that when a bias comparison to the SST simulation is done for the sensible heat flux, the relationship appears to be not as well matched between the variables. This finding likely means that the sensible heat flux simulation is sensitive to other variables not analyzed in this study, such as the air temperature simulation. Overall, the results shown thus far indicate that the climate simulations of Central America are highly sensitive to the choice of cumulus parameterization, as adopting RR-KF2 led to cascading changes among a multitude of climate parameters, all linked to the excessive or absent convection simulated by both models. As subsequent results show, the impact of changing the cumulus parameterization scheme spans beyond strictly the seasonal time scale, extending into other temporal scales and specific climatic features.

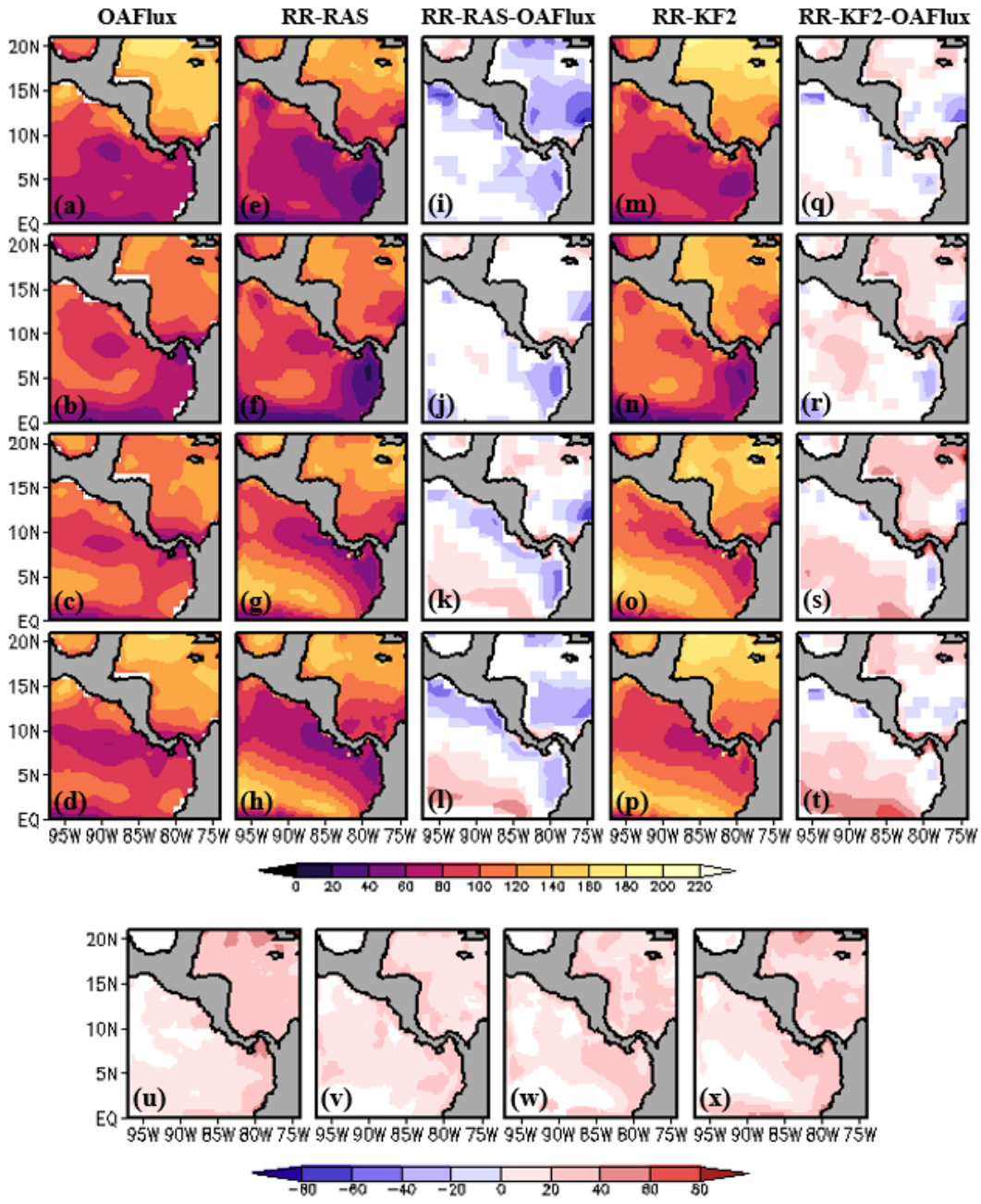

Figure 14: The seasonal mean climatological surface latent heat flux (Wm^{-2}; shaded) from (a, b, c, d) observations (OAFlux) and (e, f, g, h) RR-RAS, (I, j, k, l) systematic errors of RR-RAS, (m, n, o, p) RR-KF2, (q, r, s, t) systematic errors of RR-KF2 and (u, v, w, x) difference of (RR-KF2) – (RR-RAS). The differences in (u, v, w, x) are shaded only if they exceed 95% confidence interval.

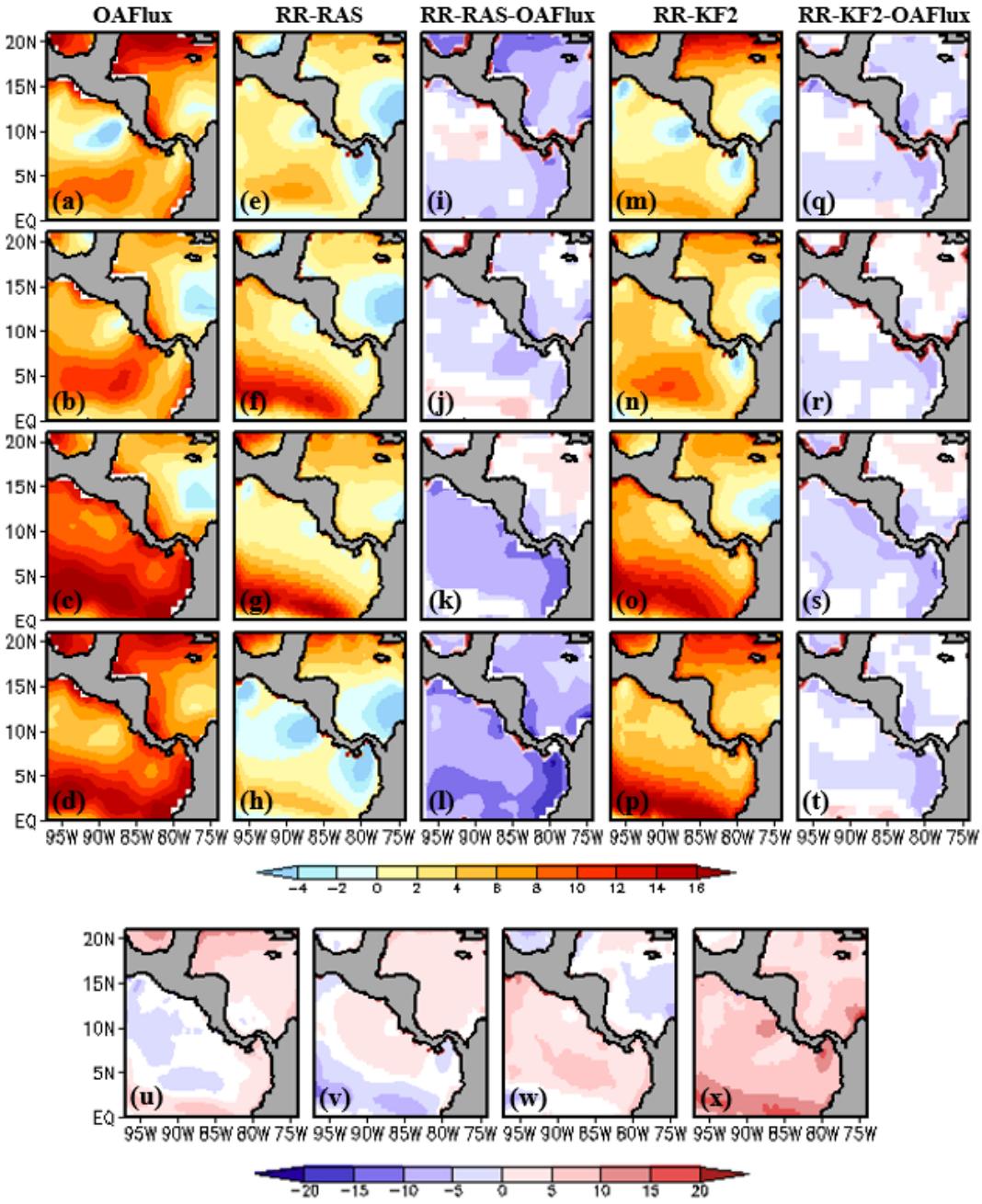

Figure 15: The seasonal mean climatological surface sensible heat flux (Wm^{-2}; shaded) from (a, b, c, d) observations (OAFlux) and (e, f, g, h) RR-RAS, (I, j, k, l) systematic errors of RR-RAS, (m, n, o, p) RR-KF2, (q, r, s, t) systematic errors of RR-KF2 and (u, v, w, x) difference of (RR-KF2) – (RR-RAS). The differences are shaded in (u, v, w, x) only if they exceed 95% confidence interval.

3.2 Diurnal Variability of Precipitation

The local diurnal harmonic is isolated following Dai and Wang (1999). The harmonic analysis of a timeseries is done by the decomposition of a periodic function into a sum of trigonometric functions like:

$$R(t) = R_o + \sum_{i=1}^{N/2} A_i cos(i\theta - \Phi_i) - - - - - - - - - (1)$$

Where, N, R_o, A_i, Φ_i are the number of intervals (=24 for hourly), daily mean value of the variable, amplitude, and phase angle of the i[th] harmonic (with i=1 corresponding to diurnal harmonic), and $\theta = \frac{2\pi t_k}{N}, t_k = \{00, 01, 02, 03, \ldots .24\}$, respectively. This analysis was done since there is a growing consensus that a good simulation of the diurnal cycle is necessary for representing the regional climate of the region (Yang and Slingo 2001; Diro et al. 2012; Martinez-Castro et al. 2018). The results of Curtis (2004) and Diro et al. (2012) mentioned previously are reaffirmed by the half-hourly IMERG observations in Figs. 16 and 17 for the JJA and SON seasons, respectively.

In JJA, the IMERG observations in Fig. 16a indicate that the diurnal amplitude of rainfall is over 6 mm/day across Central America, except for a transect from western Nicaragua through northern Honduras containing values below 6 mm/day. Interestingly, the oceans just west of Colombia exhibit a strong diurnal amplitude with rain rates over 27 mm/day, aligning with the findings of Poveda and Mesa (2000), identifying this region as one of the rainiest locales on Earth. However, Shige et al. (2017) suggest that infrared-based rainfall estimates used in the IMERG rainfall dataset tend to erroneously smear rainfall in the coastal oceans upstream of orography, bringing into question their use in coastal mountainous regions. Furthermore, the amplitude of the rainfall over the eastern Pacific Ocean and in the Mosquito Gulf in the Caribbean Sea have diurnal amplitudes exceeding 13 mm/day, the eastern Pacific Ocean displaying a clear signal of elevated amplitudes corresponding to the east Pacific ITCZ. The corresponding simulations from RR-RAS (Fig. 16b) and RR-KF2 (Fig. 16c) show close correspondence to the observations (Fig. 16a). Although, both models show a tendency to overestimate the diurnal amplitude over the terrestrial regions and underestimate over the neighboring oceans. These patterns in the diurnal amplitude simulation reflect previous results of the surface precipitation climatology, with the overestimation of terrestrial diurnal rainfall amplitude reflecting the terrestrial wet bias of RR-RAS and RR-KF2

(Figs. 4 and 16). Furthermore, the diurnal rainfall amplitudes over the east Pacific ITCZ being weaker and displaced toward the northeast reflects the ITCZ biases previously discussed, with RR-KF2 also simulating weaker diurnal rainfall amplitudes for the ITCZ compared to RR-RAS.

The corresponding verification of the phase of the diurnal cycle of precipitation in Figs. 16d-f suggests that the models are doing a reasonable job of simulating this feature. For example, the contrast in the peak of the diurnal rainfall over the eastern Pacific Ocean and the terrestrial Central America is picked quite well in both model simulations. However, both models show a tendency for the peak diurnal rainfall to occur in the early morning hours in Honduras, El Salvador, and Guatemala and along the coasts of Colombia. The results are very similar for SON (Fig. 17). In both these seasons, however, the differences in the diurnal variations of precipitation between the two models appear insignificant.

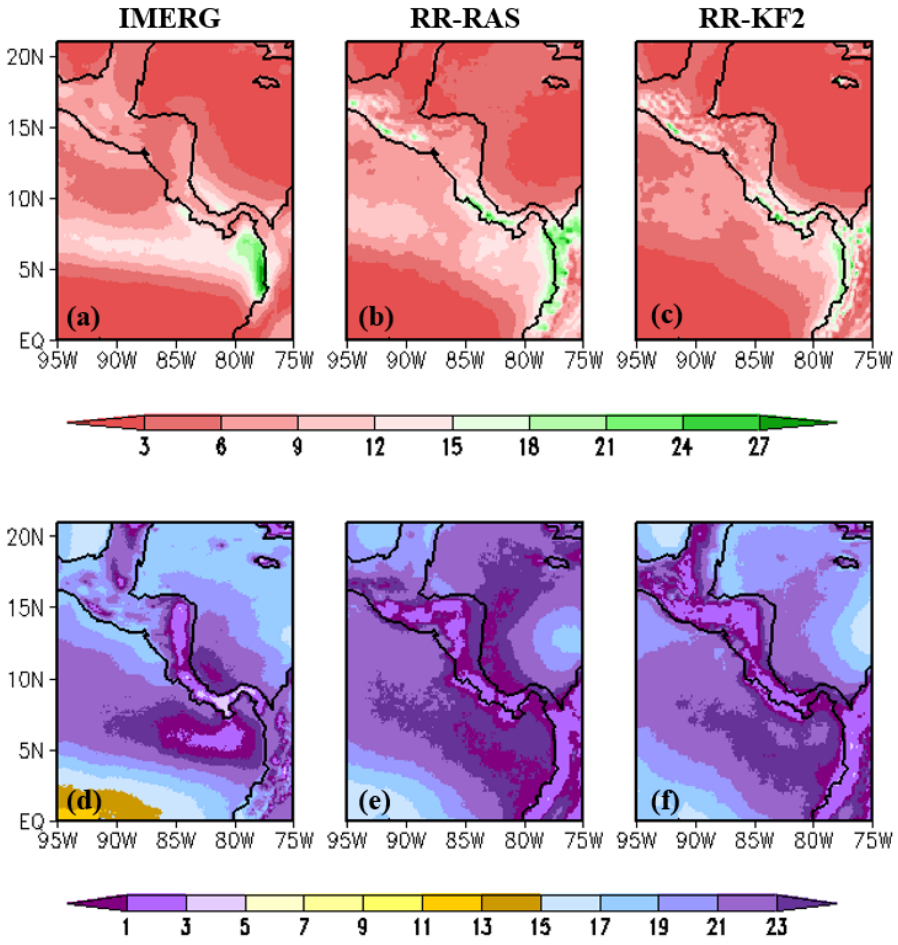

Figure 16: The mean JJA climatological (a, b, c) diurnal amplitude (mm/day) and (d, e, f) phase of rainfall (LST) from (a, d) observations (IMERG), (b, e) RR-RAS, and (c, f) RR-KF2.

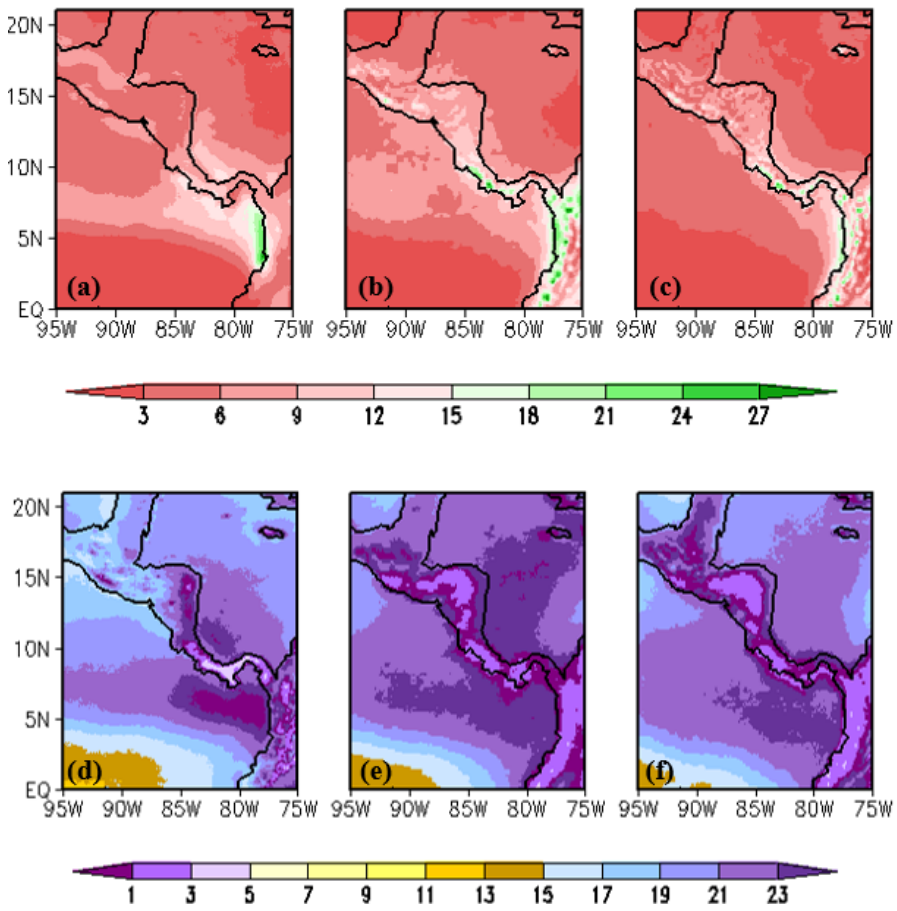

Figure 17: The mean SON climatological (a, b, c) diurnal amplitude (mm/day) and (d, e, f) phase of rainfall (LST) from (a, d) observations (IMERG), (b, e) RR-RAS, and (c, f) RR-KF2.

3.3 Mid-Summer Drought

In the results of Fig. 18, the intensity of the MSD is defined as the difference between the average of the biannual peaks of rainfall and the average of rainfall in the intervening months between the biannual peaks. This definition matches the findings of Poveda and Mesa (2000), which identified the MSD as a local minima of rainfall of any degree during July and August, between the wet season peaks in June and September (Poveda and Mesa 2000). Furthermore, the frequency of its occurrence is defined as the fraction of seasons with MSD in 15 years (1986-2001). As noted earlier, IMERG shows the amplitude of MSD to be largest over the Central American Corridor, with a relative minimum along the Caribbean coast (Fig. 18a). This pattern is also apparent in the frequency of MSD, the highest and lowest frequency appearing along the Pacific and Caribbean coasts, respectively, consistent with the idea that the MSD is a phenomenon

restricted to the Pacific coast of Central America. Both models produce similar features effectively but also over-amplify the amplitude of MSD and underestimate the frequency compared to IMERG observations, with seemingly insignificant differences between the models. Once again, biases tied to MSD amplitude and frequency are likely tied to terrestrial wet bias, as excessive rainfall would clash with the defined parameters for the MSD events.

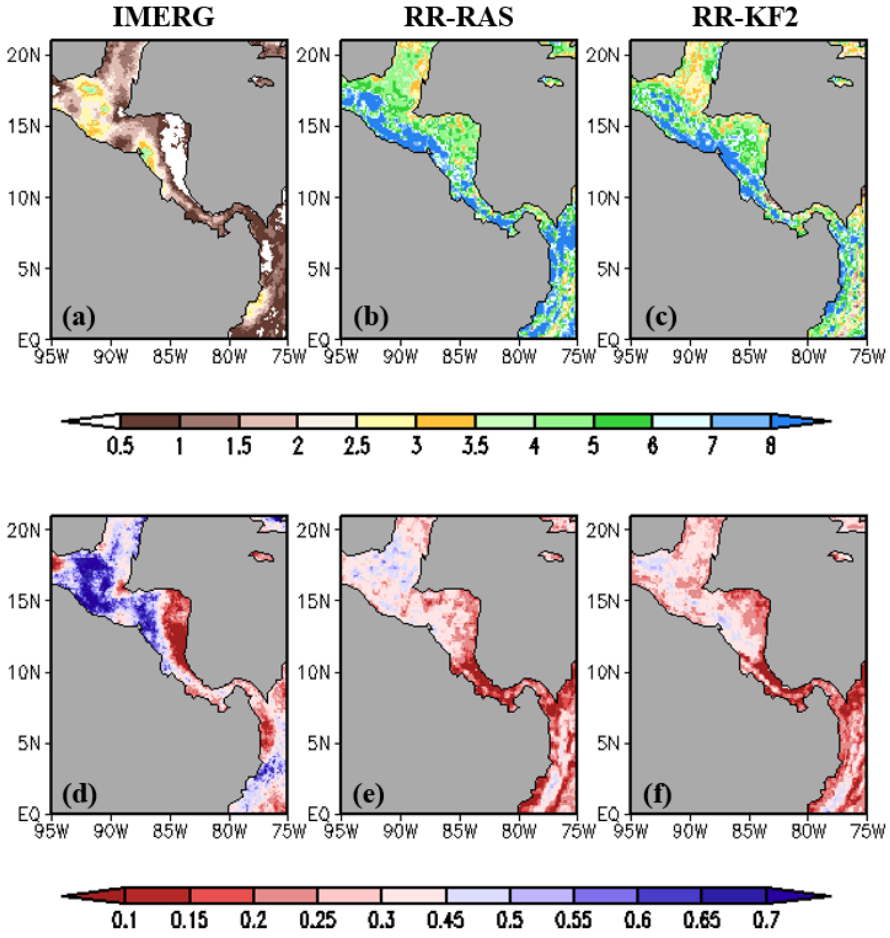

Figure 18: The (a, b, c) intensity (I; units: mm day^{-1}) and (d, e, f) frequency (F; fraction of events in 15 years: 1986–2001) of the mid-summer drought events from (a, d) IMERG, (b, e) RR-RAS, and (c, f) RR-KF2.

CHAPTER 4

CONCLUSIONS

The isthmus of Central America stands as a significant challenge in climate modeling due to the various features that simultaneously influence the regional climate and each other. Steep orography divides the narrow terrestrial region in half, allowing for unique interactions with the seasonally changing trade winds and surrounding tropical oceans, which display their own variability. These interactions between the air, sea, and land allow for year-round convective activity and some of the rainiest locales in the world to exist, making precipitation a focal point of the Central American climate. Due to its higher resolution, regional climate modeling provides an opportunity to incorporate these climatological features to enable accurate climate simulation. However, earlier studies that used regional climate models in Central America have been conducted solely with an atmospheric component, leaving out key air-sea interactions. This work is unique because a regional coupled ocean-atmosphere model was used to examine the sensitivity of climate simulations of Central America to cumulus parameterization schemes. In such a framework, where the ocean and atmosphere are co-evolving, the differences in the model simulations between the two cumulus parameterization schemes also reflect the coupled air-sea feedback that is part of the real-world climate variations, making this work key to understanding the importance of simulating air-sea interactions and convection for studying Central America's climate.

In this study, two commonly used and conceptually different cumulus parameterization schemes, RAS and KF2, were tested in a coupled ocean-atmosphere model (RSM-ROMS) at a resolution of 15 km grid spacing over a 16-year integration. The RAS scheme is based on quasi-equilibrium theory, where convection maintains a quasi-equilibrium by stabilizing the atmospheric column as it is destabilized by large-scale processes. On the other hand, in KF2, convection is triggered when a threshold of CAPE and moisture convergence is reached. The regional climate simulation of Central America, within the RSM-ROMS model forced by the global reanalysis of the atmosphere and the ocean, proved highly sensitive to the cumulus parameterization schemes. The RR-KF2 simulation showed a tendency to reduce the terrestrial wet bias, the dry bias of the atmospheric column over the oceans, the westerly bias of the low-level trades in the Caribbean Sea, and the cold coastal SST bias relative to RR-RAS. The alleviation of the cold coastal SST

bias in RR-KF2 specifically can likely be attributed to two factors, cloud radiative effects enabling surface warming and increased mixing in the oceans. Additionally, RR-KF2 improved upon the northward ITCZ bias, initiation of convective precipitation within terrestrial and coastal areas, the simulation of the Choco Jet, thermoclines in both ocean basins, and the generation of upward surface latent and sensible heat fluxes. The progress brought by RR-KF2 largely coincides with the results of the Taylor Diagrams, in which the greatest improvements in standard deviations and pattern correlations were seen among the seasonal terrestrial surface precipitation, SSTs, and thermocline depth climatology.

Furthermore, the diurnal variations of precipitation and the Mid-Summer Drought phenomenon were comparable in the two regional model simulations. The diurnal variations of precipitation in the boreal summer and fall seasons in RR-RAS and RR-KF2 had reasonable amplitude and phase compared to observations. Similarly, the qualitative properties of the Mid-Summer Drought were reasonably replicated, with the Caribbean coast showing a smaller amplitude and frequency than the Pacific coast of Central America. However, the model simulations over-amplified the bi-annual peaks of the rainfall compared to the observations, leading to an over-amplified Mid-Summer Drought.

The overall improvements in the RR-KF2 simulation relative to RR-RAS are an encouraging development for the climate simulation of Central America. However, there are features in the RR-KF2 simulation that still require further improvement, such as its weak ITCZ, wet bias over the terrestrial regions of the domain, lack of stratiform precipitation within areas of deep convection or open ocean, incorrect position of the LLJ cores, warm SST biases over portions of the east Pacific and Caribbean Sea, and shallow thermocline depths. Much of the biases seen in RR-RAS and RR-KF2 are likely connected to the convection thresholds used by both models failing to accurately interact with the climatological conditions of Central America. Therefore, future modeling work should focus on using a systematic approach of testing different cumulus parametrization schemes or convection thresholds within twin experiments to investigate what produces the most accurate precipitation climatology, which could lead to an overall improvement in the simulation of Central America’s climate.

REFERENCES

Alfaro, E. J. (2002). Some characteristics of the annual precipitation cycle in Central America and their relationships with its surrounding tropical oceans. *Tópicos Meteorológicos y Oceanográficos*, *9*(2), 88-103.

Alfaro, E. J., X. Chourio, A. G. Muñoz, and S. J. ´ Mason, 2018: Improved seasonal prediction skill of rainfall for the Primera season in Central America. Int. J. Climatol., 38, e255–e268, https://doi. org/10.1002/joc.5366.

Almazroui, M., Islam, M.N., Saeed, F. et al. Projected Changes in Temperature and Precipitation Over the United States, Central America, and the Caribbean in CMIP6 GCMs. Earth Syst Environ 5, 1–24 (2021). https://doi.org/10.1007/s41748-021-00199-5

Alpert, J., M. Kanamitsu, P. Caplan, J. Sela, and G. White, 1988: Mountain induced gravity wave drag parameterization in the NMC medium-range forecast model. In Conference on Numerical Weather Prediction, 8th, Baltimore, MD. 726-733.

Amador, J. A., Alfaro, E. J., Lizano, O. G., & Magaña, V. O. (2006). Atmospheric forcing of the eastern tropical Pacific: A review. *Progress in Oceanography*, *69*(2–4), 101–142. https://doi.org/10.1016/j.pocean.2006.03.007

Amador, J. A. (2008). The Intra-Americas Sea low-level jet: Overview and future research. *Annals of the New York Academy of Sciences*, *1146*, 153–188. https://doi.org/10.1196/annals.1446.012

Baldwin, J. W., Atwood, A. R., Vecchi, G. A., & Battisti, D. S. (2021). Outsize influence of Central American orography on global climate. *AGU Advances*, *2*(2), e2020AV000343.

Cabos, W., Sein, D.V., Durán-Quesada, A., Liguori, G., Koldunov, N. V., Martínez-López, B., Alvarez, F., Sieck, K., Limareva, N. and Pinto, J.G. (2019) Dynamical downscaling of historical climate over CORDEX Central America domain with a regionally coupled atmosphere-ocean model. Climate Dynamics, 52, 4305-4328.

Carton, J. A., & Giese, B. S. (2008). A reanalysis of ocean climate using Simple Ocean Data Assimilation (SODA). Monthly Weather Review, 136, 2999–3017. https://doi.org/10.1175/2007MWR1978.1

Castro-Martinez, D., and coauthors, 2018: The performance of RegCM4 over Central America and the Caribbean region using different cumulus parameterizations. Clim. Dyn., 50, 4103-4126, doi:10.1007/s00382-017-3863-y.

Cavazos, T., R. Luna-Nino, R. Cerezo-Mota, R. Fuentes-Franco, M. Mendez, L. F. P. Martinez, and E. Valenzuela, 2020: Climatic trends and regional climate models intercomparison over the CORDEX-CAM (Central America, Caribbean, and Mexico) domain. Int. J. Climatol., doi:10.1002/joc.6276.

Chou, M. D., & Suarez, M. J. (1994). An efficient thermal infrared radiation parameterization for use in general circulation models. NASA Technical Memorandum NASA-TM-104606, 3, 98. Retrieved from https://ntrs.nasa.gov/archive/nasa/casi.ntrs.nasa.%20gov/19950009331.pdf

Chou, M. D., & Lee, K. T. (1996). Parameterizations for the absorption of solar radiation by water vapor and ozone. Journal of the Atmospheric Sciences, 53, 1203–1208. https://doi.org/10.1175/1520-0469(1996)0532.0.co;2

Corrales-Suastegui, A., Fuentes-Franco, R., & Pavia, E. G. (2020). The mid-summer drought over Mexico and Central America in the 21st century. *International Journal of Climatology*, *40*(3), 1703-1715.

Curtis, S. (2004). Diurnal cycle of rainfall and surface winds and the mid-summer drought of Mexico/Central America. *Climate Research*, *27*(1), 1-8.

Dai A, Wang J (1999) Diurnal and semidiurnal tides in global surface pressure fields. J. Atmos. Sci., 56, 3874-3891.

Davis, R. E., Hayden, B. P., Gay, D. A., Phillips, W. L., & Jones, G. V. (1997). The north atlantic subtropical anticyclone. *Journal of Climate*, *10*(4), 728-744.

Diro, G. T., Rauscher, S. A., Giorgi, F., & Tompkins, A. M. (2012). Sensitivity of seasonal climate and diurnal precipitation over Central America to land and sea surface schemes in RegCM4. *Climate Research*, *52*(1), 31–48. https://doi.org/10.3354/cr01049

Durán-Quesada, A. M., Gimeno, L., & Amador, J. (2017). Role of moisture transport for Central American precipitation. *Earth System Dynamics*, *8*(1), 147-161.

Emanuel, K. A. (1994). *Atmospheric convection*. Oxford university press.

Ek, M. B., K. E. Mitchell, Y. Lin, E. Rogers, P. Grunmann, V. Koren, G. Gayno, J. D. Tarpley, 2003: Implementation of Noah land surface model advances in the National Centers for Environmental Prediction operational mesoscale Eta model. Journal of Geophysical Research: Atmospheres. 108(D22).

Ezer, T., H. Arango, and A. F. Shchepetkin, 2002: Developments in terrain-following ocean models: intercomparisons of numerical aspects. Ocean Modelling, 4, 249-267.

Fiedler, P. C. (2002). The annual cycle and biological effects of the Costa Rica Dome. In *Deep-Sea Research I* (Vol. 49).

Garreaud, R., & Wallace, J. M. (1997). The diurnal march of convective cloudiness over the Americas. *Monthly Weather Review*, *125*(12), 3157-3171.

Gotlieb, Y., Pérez-Briceño, P. M., Hidalgo, H., & Alfaro, E. (2019). The Central American Dry Corridor: a consensus statement and its background. *Revista Yu'am*, *3*(5), 42-51.

Haidvogel, D. B., H. G. Arango, K. Hedstrom, A. Beckmann, P. Malanotte-Rizzoli, A. F. Shchepetkin, 2000: Model evaluation experiments in the North Atlantic Basin: simulations in nonlinear terrain-following coordinates. Dynamics of atmospheres and oceans. 32(3):239-81.

Ham, S., Yoshimura, K., & Li, H. (2016). Historical dynamical downscaling for East Asia with the atmosphere and ocean coupled regional model. Journal of the Meteorological Society of Japan, 94A, 199–208. https://doi.org/10.2151/jmsj.2015-046.

Hastenrath, S., & Polzin, D. (2013). Climatic variations in Central America and the Caribbean. *International Journal of Climatology*, *33*(6), 1348–1356. https://doi.org/10.1002/joc.3515

Hersbach, H., W. Bell, P. Berrisford, A. Horanyi, J. M. Sabater, J. Nicolas, C. Peubey, R. Radu, D. Schepers, A. Simmons, C. Soci, S. Abdalla, X. Abellan, G. Balsamo, P. Bechtold, G. Biavati, J. Bidlot, M. Nonavita, G. De Chiara, P. Dahlgren, D. Dee, M. Diamantakis, R. Dragani, J. Flemming, R. Forbes, M. Fuentes, A. Geer, L. Jaimberger, S. Healy, R. J. Hogan, E. Holm, M. Janiskova, S. Keeley, P. Laloyaux, P. Lopez, C. Lupu, G. Radnoti, P. de Rosnay, I. Rozum, F. Vamborg, S. Villaume, J. -N. Thepaut, 2019: The ERA5 global reanalysis. Quart. Roy. Met. Soc., https://doi.org/10.1002/qj.3803

Hidalgo, H. G., Durán-Quesada, A. M., Amador, J. A., & Alfaro, E. J. (2015). The caribbean low-level jet, the inter-tropical convergence zone and precipitation patterns in the intra-Americas Sea: A proposed dynamical mechanism. *Geografiska Annaler, Series A: Physical Geography*, *97*(1), 41–59. https://doi.org/10.1111/geoa.12085

Hidalgo, H. G., Alfaro, E. J., Amador, J. A., & Bastidas, Á. (2019). Precursors of quasi-decadal dry-spells in the Central America Dry Corridor. *Climate Dynamics*, *53*, 1307-1322.

Hidalgo, H. G., Alfaro, E. J., Hernãandez-Castro, F., & Pérez-Briceño, P. M. (2020). Identification of tropical cyclones' critical positions associated with extreme precipitation events in central america. *Atmosphere*, *11*(10). https://doi.org/10.3390/atmos11101123

Hong, S. Y. and H. L. Pan, 1996: Nonlocal boundary layer vertical diffusion in a medium-range forecast model. Monthly weather review, 124(10):2322-2339.

Houze Jr, R. A. (1997). Stratiform precipitation in regions of convection: A meteorological paradox?. *Bulletin of the American Meteorological Society*, *78*(10), 2179-2196.

Huffman, G. J., E. F. Stocker, D. T. Bolvin, E. J. Nelkin, and J. Tan, 2019: GPM IMERG final precipitation L3 half hourly 0.1 degree 3 0.1 degree V06 at GES DISC. Goddard Earth Sciences Data and Information Services Center (GES DISC), accessed 7 July 2021, https://doi.org/10.5067/GPM/IMERG/ 3B-HH/06.

Juang, H. M., & Kanamitsu, M. (1994). The NMC nested regional spectral model. Monthly Weather Review, 122, 3–26. https://doi.org/10.1175/ 1520-0493(1994)1222.0.co;2.

Kain, J., and M. Fritsch (1993), Convective parameterization for mesoscale models: The Kain-Fritsch scheme, Meteorol. Monogr., 24, 165–170.

Kanamitsu, M., Ebusuzaki, W., Woollen, J., Yang, S.-K., Hnilo, J., Fiorino, M., & Potter, G. L. (2002). NCEP-DOE AMIP-II reanalysis (R-2). Bulletin of the American Meteorological Society, 83, 1631–1643. https://doi.org/10.1175/bams-83-11-1631(2002)0832.3.co;2

Kanamitsu, M., K. Yoshimura, B. Y. Yhang, S. Y. Hong, 2010: Errors of interannual variability and trend in dynamical downscaling of reanalysis. Journal of Geophysical Research: Atmospheres. 115(D17).

Kane, J. S., 2004: The Kane-Fritsch convective parameterization: An update. J. Appl. Met. and Climatol., 43, 170-181.

Kowal, K. M., L. J. Slater, A. G. Lopez, and A. F. Van Loon, 2023: A comparison of seasonal rainfall forecasts over Central America using dynamic and hybrid approaches from Copernicus Climate Change Service seasonal forecasting system and the North American Multimodel Ensemble. Int. J. Climatol., https://doi.org/10.1002/joc7969.

Large, W. G., and J. C. McWilliams, and S. C. Doney, 1994: Oceanic vertical mixing: A review and a model with a nonlocal boundary layer parameterization. Reviews of Geophysics, 32(4):363-403.

L'Ecuyer, T. S., Hang, Y., Matus, A. V., & Wang, Z. (2019). Reassessing the effect of cloud type on Earth's energy balance in the age of active spaceborne observations. Part I: Top of atmosphere and surface. *Journal of Climate*, *32*(19), 6197-6217.

Li, H., Kanamitsu, M., Hong, S. Y., Yoshimura, K., Cayan, D. R., & Misra, V. (2014). A high-resolution ocean-atmosphere coupled downscaling of the present climate over California. *Climate Dynamics*, *42*, 701-714.

Li, H. and Misra, V. (2014) Thirty-two-year ocean–atmosphere coupled downscaling of global reanalysis over the Intra-American Seas. Climate Dynamics, 43, 2471–2489. https://doi.org/10.1007/s00382-014-2069-9.

Magan˜a, V., Magan˜a, M., Amador, J. A., & Medina, S. (1999). *The Midsummer Drought over Mexico and Central America*.

Mapes, B. E., Warner, T. T., Xu, M., & Negri, A. J. (2003). *Diurnal Patterns of Rainfall in Northwestern South America. Part I: Observations and Context*.

Mapes, B. E., Warner, T. T., & Xu, M. (2003). Diurnal patterns of rainfall in northwestern South America. Part III: Diurnal gravity waves and nocturnal convection offshore. *Monthly weather review*, *131*(5), 830-844.

Mapes, B. E., T. T. Warner, M. Xu, and D. J. Gochis, 2004: Comparison of cumulus parameterizations and entrainment using domain-mean wind divergence in a regional model. J. Climate, 61, 1284-1295, https://doi.org/10.1175/1520-0469(2004)061<1284:COCPAE>2.0.CO;2

María Durán-Quesada, A., Gimeno, L., & Amador, J. (2017). Role of moisture transport for Central American precipitation. *Earth System Dynamics*, *8*(1), 147–161. https://doi.org/10.5194/esd-8-147-2017

Martinez-Castro, D., and coauthors, 2018: The performance of RegCM4 over the Central America and Caribbean region using different cumulus parameterizations. Clim. Dyn., 50, 4103-4126.

Mellor, G.L., Yamada, T., 1982. Development of a turbulence closure model for geophysical fluid problems. Rev. Geophys. 20 (4), 851–875.

Misra, V., Li, H., & Kozar, M. (2014). The precursors in the Intra-Americas Seas to seasonal climate variations over North America. *Journal of Geophysical Research: Oceans*, *119*(5), 2938-2948.

Misra, V., Mishra, A., & Bhardwaj, A. (2018). Simulation of the intraseasonal variations of the Indian summer monsoon in a regional coupled ocean–atmosphere model. *Journal of Climate*, *31*(8), 3167-3185.

Misra, V. and C. B. Jayasankar, 2022: A high resolution coupled ocean-atmosphere simulation of the regional climate over Central America Clim. Dyn., https://doi.org/10.1007/s00382-021-06083-2.

Moorthi, S., & Suarez, M. J. (1992). Relaxed Arakawa-Schubert. A parameterization of moist convection for general circulation models. Monthly Weather Review, 120(6), 978–1002. https://doi.org/10.1175/1520-0493(1992)1202.0.co;2

Mora, Gabriela. (2017). Climatology of the low-level winds over the Intra-Americas sea using satellite and reanalysis data. 16. Available from https://www.researchgate.net/profile/Gabriela-Mora-7/publication/325766427_Climatology_of_the_low-level_winds_over_the_intraamericas_sea_using_satellite_and_reanalysis_data/links/5b22a8f4458515270fcb6413/Climatology-of-the-low-level-winds-over-the-intraamericas-sea-using-satellite-and-reanalysis-data.pdf

Muñoz, E., Busalacchi, A. J., Nigam, S., & Ruiz-Barradas, A. (2008). Winter and summer structure of the Caribbean low-level jet. *Journal of Climate*, *21*(6), 1260–1276. https://doi.org/10.1175/2007JCLI1855.1

Poveda, G., & Mesa, O. J. (2000). On the existence of Lloró (the rainiest locality on earth): Enhanced ocean-land-atmosphere interaction by a low-level jet. *Geophysical Research Letters*, *27*(11), 1675–1678. https://doi.org/10.1029/1999GL006091

Reynolds, R. W., T. M. Smith, C. Liu, D. B. Chelton, K. S. Casey, and M. G. Schlax, 2007: Daily high-resolution-blended analyses for sea surface temperature. *Journal of Climate*, 20, 5473–5496, doi:10.1175/JCLI-D-14-00293.1.

Rodgers, J., V. Misra, and C. B. Jayasankar, 2024:Using the Observed Variations of the Start Date of the Rainy Season over Central America for its Reliable Seasonal Outlook J. Climate, https://doi.org/10.1175/JCLI-D-23-0699.1

Sáenz, F., Hidalgo, H. G., Muñoz, Á. G., Alfaro, E. J., Amador, J. A., & Vázquez-Aguirre, J. L. (2023). Atmospheric circulation types controlling rainfall in the Central American Isthmus. *International Journal of Climatology*, *43*(1), 197–218. https://doi.org/10.1002/joc.7745

Schumacher, C., & Houze Jr, R. A. (2003). Stratiform rain in the tropics as seen by the TRMM precipitation radar. *Journal of climate*, *16*(11), 1739-1756.

Schumacher, C., & Funk, A. (2023). Assessing convective-stratiform precipitation regimes in the tropics and extratropics with the GPM satellite radar. *Geophysical Research Letters*, *50*(14), e2023GL102786.

Shchepetkin, A. F., & McWilliams, J. C. (2005). The regional oceanic modeling system (ROMS): A split-explicit, free-surface, topography-following-coordinate oceanic model. Ocean Modelling, 9(4), 347–404. https://doi.org/10.1016/j.ocemod.2004.08.002

Shige, S., Nakano, Y., & Yamamoto, M. K. (2017). Role of orography, diurnal cycle, and intraseasonal oscillation in summer monsoon rainfall over the Western Ghats and Myanmar Coast. *Journal of Climate*, *30*(23), 9365-9381.

Stewart, I. T., Maurer, E. P., Stahl, K., & Joseph, K. (2022). Recent evidence for warmer and drier growing seasons in climate sensitive regions of Central America from multiple global datasets. *International Journal of Climatology*, *42*(3), 1399-1417.

Tatsumi, Y. (1986). A spectral limited-area model with time-dependent lateral boundary conditions and its application to a multi-level primitive equation model. *Journal of the Meteorological Society of Japan. Ser. II*, *64*(5), 637-664.

Taylor, K. E. (2001). Summarizing multiple aspects of model performance in a single diagram. *Journal of Geophysical Research Atmospheres*, *106*(D7), 7183–7192. https://doi.org/10.1029/2000JD900719

Tiedtke, M., 1983: The sensitivity of the time-mean large-scale flow to cumulus convection in the ECMWF model. In: Proceedings of ECMWF Workshop on Convective in Large-scale Models. European Centre for Medium-Range Weather Forecasts, Reading, United Kingdom. 297–316.

Torres-Alavez, J. A., Das, S., Corrales-Suastegui, A., Coppola, E., Giorgi, F., Raffaele, F., ... & Sines, T. (2021). Future projections in the climatology of global low-level jets from CORDEX-CORE simulations. *Climate Dynamics*, 1-19.

Umlauf, L. and H. Burchard, 2003: A generic length-scale equation for geophysical turbulence models. Journal of Marine Research. 61(2):235-65.

Vera, C., Higgins, W., Amador, J., Ambrizzi, T., Garreaud, R., Gochis, D., Gutzler, D., Lettenmaier, D., Marengo, J., Mechoso, C. R., Nogues-Paegle, J., Dias, P. L. S., & Zhang, A. C. (2006). *Toward a Unified View of the American Monsoon Systems*.

Wang, C., & Enfield, D. B. (2001). The tropical western hemisphere warm pool. *Geophysical Research Letters*, *28*(8), 1635–1638. https://doi.org/10.1029/2000GL011763

Wang, P. X., Wang, B., Cheng, H., Fasullo, J., Guo, Z. T., Kiefer, T., & Liu, Z. Y. (2014). The global monsoon across timescales: coherent variability of regional monsoons. *Climate of the Past*, *10*(6), 2007-2052.

Xie, S. and Coauthors, 2002: Intercomparison and evaluation of cumulus parameterizations under summertime midlatitude continental conditions. Quart. Roy. Met. Soc., 128, 1095-1135.

Yang G, Slingo J (2001) The diurnal cycle in the tropics. Mon Weather Rev 129: 784−801.

Yepes, J., G. Poveda, J. F. Mejia, L. Moreno, and C. Rueda, 2019: CHOCO-JEX: A research experiment focused on the Choco Low-Level Jet over the far Eastern Pacific and Western Colombia. Bull Amer. Soc., 18, 779-796, https://doi.org/10.1175/BAMS-D-18-0045.1

Yu L, Jin X, Weller RA. 2008. Multidecade global flux datasets from the Objectively analyzed Air-sea Fluxes (OAFlux) Project: latent and sensible heat fluxes, ocean evaporation, and related surface meteorological variables. OAFlux Project Technical Report OA-2008-01, Woods Hole Oceanographic Institution, Woods Hole, MA, 64 pp.

Zhao, Q. and F. H. Carr, 1997: A prognostic cloud scheme for operational NWP models. Monthly Weather Review. 125(8):1931-1953.

BIOGRAPHICAL SKETCH

Justin Gonzalez was born and raised in Miami, Florida, where he first attended Miami Dade Honors College. During his time in this institution, he worked on multiple honors research projects in collaboration with several faculty members, which included topics such as the physical processes involved in tropical cyclogenesis and the influence of orographic lift in lightning formation. After completing his Associate of Arts in Atmospheric Sciences and Meteorology in August of 2021, he transferred to Florida State University to complete his undergraduate education. Upon entering Florida State University, he continued his research work through the Undergraduate Research Opportunity Program (UROP), in which he worked with Dr. Hannah Hiester on a project concerning the most beneficial design elements for STEM video education. He would later become a Florida Georgia Louis Stokes Alliance for Minority Participation (FGLSAMP) recipient, where he sharpened his leadership skills and gained guidance in the transition to graduate school. After receiving his Bachelor of Science in Meteorology in May of 2023, he began attending graduate school at Florida State University to work toward a Master of Science in Meteorology. During graduate school, he worked as a teaching assistant for introductory meteorology courses and volunteered for the Tallahassee branch of the National Weather Service. The results shown in his master's thesis have been submitted to the American Meteorological Society Journal of Applied Meteorology and Climatology to publish his work.